Viscous dissipation by tidally forced inertial modes in a rotating spherical shell

M. RIEUTORD[1]† AND L. VALDETTARO[2]

[1]Laboratoire d'Astrophysique de Toulouse – Tarbes, CNRS et Université de Toulouse,
14 avenue E. Belin, 31400 Toulouse, France

[2]MOX – Dipartimento di Matematica, Politecnico di Milano, Piazza L. da Vinci,
32, 20133 Milano, Italy

We investigate the properties of forced inertial modes of a rotating fluid inside a spherical shell. Our forcing is tidal like, but its main property is that it is on the large scales. By numerically solving the linear equations of this problem, including viscosity, we first confirm some analytical results obtained on a two-dimensional model by Ogilvie (*J. Fluid Mech.*, vol. 543, 2005, p. 19); some additional properties of this model are uncovered like the existence of narrow resonances associated with periodic orbits of characteristics. We also note that as the frequency of the forcing varies, the dissipation varies drastically if the Ekman number E is low (as is usually the case). We then investigate the three-dimensional case and compare the results to the foregoing model. The three-dimensional solutions show, like their two-dimensional counterpart, a spiky dissipation curve when the frequency of the forcing is varied; they also display small frequency intervals where the viscous dissipation is independent of viscosity. However, we show that the response of the fluid in these frequency intervals is crucially dominated by the shear layer that is emitted at the critical latitude on the inner sphere. The asymptotic regime, where the dissipation is independent of the viscosity, is reached when an attractor has been excited by this shear layer. This property is not shared by the two-dimensional model where shear layers around attractors are independent of those emitted at the critical latitude. Finally, resonances of the three-dimensional model correspond to some selected least damped eigenmodes. Unlike their two-dimensional counter parts these modes are not associated with simple attractors; instead, they show up in frequency intervals with weakly contracting webs of characteristics. Besides, we show that the inner core is negligible when its relative radius is less than the critical value $0.4E^{1/5}$. For these spherical shells, the full sphere solutions give a good approximation of the flows.

Key words: rotating flows, waves in rotating fluids

1. Introduction

1.1. *The background*

The question of how close binary stars born on eccentric orbits reach a circular trajectory with synchronous orbital and spin rotation is by far not fully resolved. The process of circularization of the orbits and synchronization of rotations is thought

† Email address for correspondence: rieutord@ast.obs-mip.fr

to be the result of the tidal interaction. Tides act in two ways: they first create a tidal bulge which generates a torque leading to angular momentum exchange between the orbital motion and the spinning stars. Second, they dissipate energy through the induced fluid flows. This latter effect is important as it controls the time scale of the whole evolution process.

Thus, much work has been devoted to evaluate the efficiency of the dissipative processes, which can be triggered by tides. The first process that has been investigated is the viscous damping of the equilibrium tide; this is the tide induced by the mere deformation of equipotentials; the fluid is assumed 'attached' to these surfaces and the time dependence of the tidal distortion makes the flow (see Zahn 1966, 1977, 1992, 2008). However, this process is efficient if the viscosity is high enough, a condition which is met only by low-mass stars. Indeed, the convective envelope of these stars provides a strong damping through their turbulent viscosity. However, stars of mass larger than 1.8 solar mass have no convection in their outer layers (only in the central part). Their envelope is stably stratified. But observations do show that circularization and synchronization are also effective for these stars when they are close enough (Giuricin, Mardirossian & Mezzetti 1984, but see also the recent review of observational facts on tidal interactions between stars or between stars and planets by Mazeh 2008). The present understanding of these results is based on the idea that the radiative envelope of these stars are efficiently damping the gravity waves excited by the tides. This mechanism was first investigated by Zahn (1975) using a simplified approach with an asymptotic description of gravity modes in a non-rotating fluid. However, stars in a binary system are rotating, sometimes quite rapidly. Rotation thus appeared as an unavoidable feature. Following work of Rocca (1987, 1989) therefore included the Coriolis acceleration but as a first-order perturbation.

More recently, Witte & Savonije (1999a,b, 2001) investigated numerically the synchronization process of massive stars, fully taking into account the Coriolis force in the flow. They thus discovered the phenomenon of 'resonance locking' by which the tidal forcing excites resonantly two rotationally modified gravity modes (called gravito-inertial modes), which therefore strongly dissipate energy; the locking occurs because one mode tends to spin the star up, while the other tends to spin it down. The low frequencies of the resonant gravito-inertial modes, however, is synonymous of short-wavelength modes that are not well suited to the foregoing two-dimensional numerical calculations. This difficulty motivated Savonije & Witte (2002) to further investigate the problem with the so-called Traditional Approximation which allows a separation of the variables. However, as discussed by Gerkema *et al.* (2008), this simplification eliminates a crucial feature of these modes, namely their internal shear layers. Indeed, Dintrans, Rieutord & Valdettaro (1999) showed that gravito-inertial modes are singular in the limit of vanishing diffusivities. This property is actually shared by gravity modes and inertial modes in any configuration where variables cannot be separated (see Rieutord, Georgeot & Valdettaro 2000). The singularities come from the ill-posed nature of the mathematical problem which is of hyperbolic or mixed type with boundary conditions. At non-zero but low diffusivities, dominant singularities show up as modes confined in shear layers following attractors of characteristics (Rieutord & Valdettaro 1997; Rieutord, Georgeot & Valdettaro 2001). As far as dissipation is concerned, such modes behave very differently compared to the regular ones. Astrophysical situations being characterized by large ratios between integral and dissipation scales, it is crucial to understand the asymptotic properties of resonant-mode dissipation at vanishing viscosities and thermal diffusion.

Besides the problem of tidal interactions between stars, which is quite old, the recent discovery of many planetary systems harbouring Jupiter-like planets on orbits very

close to the central star also motivates a new examination of the tidal interaction. The novelty with planets, even of the size of Jupiter, is that they likely contain a rocky core in their central part. Even if this core is not a solid body, the transition with the surrounding envelope is likely sharp (Goodman & Lackner 2009). This makes the fluid domain like a spherical shell. In stars this domain is delineated by the Brunt–Väisälä frequency variations and may be more complex (e.g. Dintrans & Rieutord 2000).

Beyond the astrophysical problem described above, the case of resonant inertial modes is also of interest in Earth sciences in relation to the elliptic instability (e.g. Lacaze, Le Gal & Le Dizès 2005), the rotating precessing flows (e.g. Hollerbach & Kerswell 1995) or for the understanding of the dynamics of the ocean or of the atmosphere (e.g. Maas 2001; Maas & Harlander 2007). Furthermore, it has also been investigated in the context of engineering applications such as the oscillations of fuel tanks of spinning spacecrafts (see Manasseh 1996). Finally, let us mention that non-axisymmetric inertial modes also appear as the growing perturbations of a rotating fluid destabilized by thermal convection (see Zhang 1994, 1995).

As may be guessed, the full astrophysical problem is very involved and some simplifications are in order if one wishes to decipher the mechanisms controlling the asymptotic laws of dissipation at small diffusivities. Thus, following the work of Ogilvie (2005), we first investigate the case of forced singular modes in a slender toroidal shell, which is a two-dimensional approximation for a spherical shell (e.g. Rieutord, Valdettaro & Georgeot 2002). Thus doing, we can recover and extend the results of Ogilvie. We proceed then by focusing on the three-dimensional problem of the spherical shell and extend the previous work of Rieutord (1991) and Tilgner (1999). We then discuss and compare the results of two-dimensional and three-dimensional models. Some conclusions end the paper.

1.2. *The model*

We consider a viscous fluid inside a spherical shell that mimics a stellar or planetary envelope, submitted to the tides of an orbiting mass point. This tidal forcing may be condensed in the tidal potential which we write as

$$\Phi_T = \Phi_{ax} r^2 P_2(\cos\theta)\cos\omega_o t + \Phi_{nx} r^2 P_2^2(\cos\theta)\cos(2\omega_o t - 2\varphi)$$

following Zahn (1977). In this expression, ω_o is the orbital angular velocity of the point mass, (r, θ, φ) are the spherical coordinates whose origin is at the centre of the body under consideration; P_2 and P_2^2 are Legendre polynomials, while Φ_{ax} and Φ_{nx} are the amplitudes. On Earth Φ_{nx} is the amplitude of the well-known semi-diurnal tide. $\Phi_{ax} r^2 P_2(\cos\theta)\cos\omega_o t$ is the leading term coming from the eccentricity of the orbit. Although Φ_{ax} is usually smaller than Φ_{nx}, we shall discard Φ_{nx} and only consider the first term of Φ_T. This is justified by the fact that the properties of non-axisymmetric inertial modes in a spherical shell are the same as those of the axisymmetric ones as far as singularities are concerned (Rieutord *et al.* 2001). Thus all the results derived below for an axisymmetric forcing can be applied, *mutatis mutandis*, to a non-axisymmetric forcing. In another problem like the resonant interaction of inertial modes, which leads to the elliptic instability (Kerswell 2002), the non-axisymmetric terms would be essential of course.

The fluid inside the spherical shell is rotating at the spin angular velocity Ω of the star. Thus, in a frame co-rotating with the fluid, the tidal forcing is

$$\Phi_T = \Phi_{ax} r^2 P_2(\cos\theta)\cos[(\omega_o - \Omega)t].$$

The first response of a star to the tidal potential is the so-called equilibrium tide, which describes the distortion of the equipotentials. This induces a velocity field $\boldsymbol{v}_e$, which is derived from the time evolution of the equipotentials. Following Zahn (1966), this induces a radial flow of the form:

$$\boldsymbol{V}_e = \mathscr{A} r^2 P_2(\cos\theta)\sin\omega t \boldsymbol{e}_r,$$

where $\omega = \omega_o - \Omega$. As shown by Ogilvie (2005), this flow forces a dynamical response of the star through the body force

$$\boldsymbol{f} = -(\mathrm{i}\omega \boldsymbol{V}_e + 2\boldsymbol{\Omega} \times \boldsymbol{V}_e).$$

We are interested in the dynamical response of the fluid. As the general realistic case is much involved, we reduce it to the study of the response of an incompressible viscous fluid inside a spherical shell. Although much simplified, this model retains the essential feature of the low-frequency stellar modes, namely their singularities associated with attractors of characteristics (e.g. Dintrans & Rieutord 2000).

Assuming that the fluid response remains of small amplitude, we need to solve the linearized equations governing forced periodic perturbations of a viscous rotating fluid with constant density. When the length scale is the outer radius of the shell R, the time scale is $(2\Omega)^{-1}$, the equations of the non-dimensional pressure (p) and velocity perturbation ($\boldsymbol{u}$) may be written:

$$\left.\begin{aligned} \mathrm{i}\omega \boldsymbol{u} + \boldsymbol{e}_z \times \boldsymbol{u} &= -\nabla p + E\,\Delta \boldsymbol{u} + \boldsymbol{f}, \\ \nabla \cdot \boldsymbol{u} &= 0, \end{aligned}\right\} \tag{1.1}$$

where $E = \nu/2\Omega R^2$ is the Ekman number and ν is the kinematic viscosity. The non-dimensional force reads

$$\boldsymbol{f} = -V_e(r,\theta)\,(\mathrm{i}\omega \boldsymbol{e}_r + \sin\theta \boldsymbol{e}_\phi), \tag{1.2}$$

where $V_e(r,\theta) = \mathscr{A} r^2 P_2(\cos\theta)$. We complete these equations with stress-free boundary conditions. The use of stress-free boundary conditions may be surprising in the planetary case as the interface between the fluid layer and the core is a solid boundary. However, because of the nature of the fluid flows that are restricted to internal shear layers, this boundary condition has little effect on the solution as was actually found by Fotheringham & Hollerbach (1998). We give in Appendix B the scaling arguments that lead to this result.

Even thus simplified, our problem remains challenging. A further simplification, actually used many times (Maas & Lam 1995; Rieutord *et al.* 2002; Ogilvie 2005), consists in reducing the problem to two dimensions. In such a case, the spherical shell turns into a (cored) slender torus (see figure 1 and Rieutord *et al.* 2002), but the eigenvalue problem as well as the forced one (far from resonances) can be solved analytically (Rieutord *et al.* 2002; Ogilvie 2005). Although this latter simplification seems quite drastic, it may be shown that it is nevertheless relevant to equatorial regions of a thin spherical shell (e.g. Stewartson 1971; Rieutord *et al.* 2002). To bridge the gap with the work of Ogilvie (2005), we therefore first consider this two-dimensional model and then move on to the three-dimensional one.
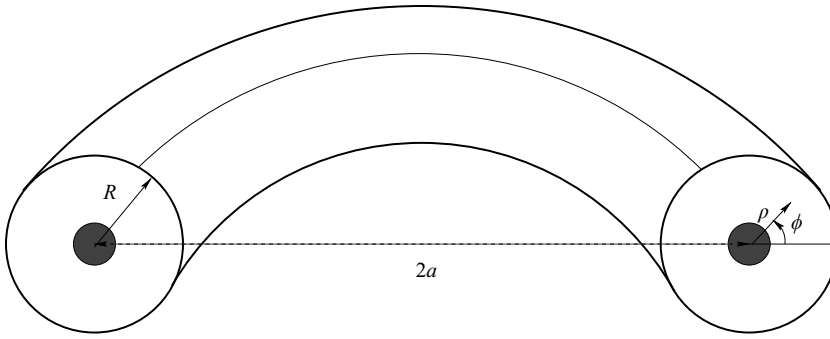
FIGURE 1. A schematic view of the slender cored torus: the principal radius a of the torus tends to infinity.

2. Resonances of axisymmetric modes in the slender torus

2.1. *Mathematical formulation*

Using cylindrical coordinates (s, φ, z), we first introduce a meridional stream function ψ so that mass conservation is automatically insured. Hence, we set

$$u_s = -\frac{\partial \psi}{\partial z}, \quad u_\varphi = u, \quad u_z = \frac{1}{s}\frac{\partial s\psi}{\partial s}.$$

The momentum equation leads to

$$\left.\begin{aligned}
E\Delta'\Delta'\psi - \partial_z u - \mathrm{i}\omega\Delta'\psi &= C, \\
E\Delta'u + \partial_z \psi - \mathrm{i}\omega u &= -f,
\end{aligned}\right\} \tag{2.1}$$

where

$$\Delta' = \Delta - 1/s^2 = \frac{\partial}{\partial s}\left(\frac{1}{s}\frac{\partial}{\partial s}s\right) + \frac{\partial^2}{\partial z^2}$$

and

$$f = f_\varphi = -\sin\theta\, V_e(r, \theta), \quad C = \frac{\partial f_s}{\partial z} - \frac{\partial f_z}{\partial s},$$

$$f_s = -\mathrm{i}\omega\sin\theta\, V_e(r, \theta), \quad f_z = -\mathrm{i}\omega\cos\theta\, V_e(r, \theta).$$

The torque density C may be further reduced into

$$C = \frac{\mathrm{i}\omega}{r}\frac{\partial V_e}{\partial \theta}.$$

System (2.1) is completed by stress-free boundary conditions which demand that

$$\psi = \frac{\partial}{\partial r}\left(\frac{1}{r}\frac{\partial \psi}{\partial r}\right) = \frac{\partial u}{\partial r} = 0 \quad \text{at} \quad r = \eta, 1.$$

Here η is the non-dimensional radius of the inner core.

2.2. *Solving the equations*

Because of the shape of the boundaries, it is natural to use polar coordinates (ρ, ϕ) in a meridional section of the torus (see the schematic view in figure 1). These coordinates are related to the foregoing cylindrical coordinates by

$$s = \rho\cos\phi, \quad z = \rho\sin\phi.$$

They are also related to the original spherical coordinates by $r = \rho$ and $\theta = \pi/2 - \phi$.

The two-dimensional approximation is essentially summarized into the neglect of the curvature terms so that, for instance, $\psi/s \ll \partial\psi/\partial s$; hence,

$$u_\rho = u_s \cos\phi + u_z \sin\phi = -\frac{1}{\rho}\frac{\partial\psi}{\partial\phi},$$

$$u_\phi = -u_s \sin\phi + u_z \cos\phi = \frac{\partial\psi}{\partial\rho}.$$

To obtain a numerical solution of the equations (2.1) (simplified with the two-dimensional-approximation), we first use a Fourier decomposition, namely

$$(\psi, u, f, C)(\rho, \phi) = \sum_n (\psi_n, -iV_n, f_n, C_n)(\rho)\,e^{in\phi},$$

and find the set of ordinary differential equations controlling the shape of the radial functions $\psi_n(\rho)$ and $V_n(\rho)$. They are

$$\left.\begin{array}{l} E\Delta_n V_n + \dfrac{\psi'_{n-1} - \psi'_{n+1}}{2} - \dfrac{(n-1)\psi_{n-1} + (n+1)\psi_{n+1}}{2\rho} - i\omega V_n = -if_n, \\[3mm] E\Delta_n\Delta_n\psi_n + \dfrac{V'_{n-1} - V'_{n+1}}{2} - \dfrac{(n-1)V_{n-1} + (n+1)V_{n+1}}{2\rho} - i\omega\Delta_n\psi_n = C_n, \end{array}\right\} \quad (2.2)$$

where

$$\Delta_n = \frac{\partial^2}{\partial\rho^2} + \frac{1}{\rho}\frac{\partial}{\partial\rho} - \frac{n^2}{\rho^2}.$$

With this formulation, the stress-free boundary conditions read

$$\psi_n = \frac{\partial^2\psi_n}{\partial\rho^2} - \frac{1}{\rho}\frac{\partial\psi_n}{\partial\rho} = \frac{\partial V_n}{\partial\rho} = 0.$$

For the tidal forcing at hands, we find that

$$\left.\begin{array}{l} f(\rho, \phi) = \dfrac{1}{2}\rho^2(\cos\phi - 2\sin^2\phi\cos\phi) = \dfrac{\rho^2}{8}(\cos\phi + 3\cos 3\phi), \\[3mm] C(\rho, \phi) = -3\,i\omega\rho\sin\phi\cos\phi \end{array}\right\} \quad (2.3)$$

so that

$$f_n = f_{-n} = \frac{\rho^2}{16}(\delta_{n,1} + 3\delta_{n,3}), \qquad C_n = -C_{-n} = -\frac{3}{4}\omega\rho\delta_{n,2}.$$

The two-dimensional set-up restricts the number of excited attractors compared to the three-dimensional one (see Rieutord *et al.* 2002 and below). Thus, although this forcing is derived from the true tidal force, we complete our view of the solutions by the use of the following forcing:

$$f(\rho, \phi) = 2\cos 2\phi, \quad C = 0;$$

thus

$$f_n = f_{-n} = \delta_{n,2}, \quad C_n = 0.$$

2.3. *Symmetries*

In modelling the tidal interaction, it is commonly assumed that spin and orbital angular momentum vectors are parallel. With this assumption, the tidal flow is symmetric with respect to the equatorial and orbital planes. In this case, the tidal force is such that $f_n = f_{-n}$ and $C_n = -C_{-n}$ as noted above.

This symmetry allows us to solve the set of equations (2.2) solely for $n \geqslant 0$. However, solutions in the torus verify a further symmetry: they may be symmetric or antisymmetric with respect to the transformation $\phi \rightarrow \phi + \pi$. Such a symmetry is specific to the torus and does not exist in the sphere. As noticed by Rieutord *et al.* (2002), it has a selection effect on attractors: some may exist in the spherical shell but be not authorized in the torus. For this reason, some attractors of the spherical shell cannot be studied in two dimensions with the natural forcing (2.3), but can be investigated with the second forcing. Still some others cannot be studied in two dimensions altogether.

The equatorial symmetry of the tidal forcing in combination with the parity of its Fourier component, implies that only half of the Fourier components are excited, namely

$$V_1, V_3, \ldots, V_{2n+1}, \ldots \quad \psi_2, \ldots, \psi_{2n} \ldots;$$

we also note that, since $V_{-1} = V_1$,

$$\Delta \Delta \psi_0 - i \omega \Delta \psi_0 = 0,$$

which means that ψ_0 is not excited and therefore vanishes. The second forcing excites the other set of Fourier components, namely

$$V_0, V_2, \ldots, V_{2n}, \ldots \quad \psi_1, \ldots, \psi_{2n+1} \ldots.$$

2.4. *Dissipation*

As discussed in the introduction, total viscous dissipation of the fluid volume is the actual quantity to be evaluated when the solution is known (this is the quantity which controls the secular evolution of the orbit). As noted by Ogilvie (2005), dissipation may be evaluated in two ways:

$$D = \frac{E}{2} \int_{(V)} |c|^2 \, dV = \int_{(V)} Re(\boldsymbol{u}^* \cdot \boldsymbol{f}) \, dV, \tag{2.4}$$

where $[\boldsymbol{c}]$ is the rate-of-strain tensor. We use both of these expressions to evaluate the internal numerical precision of our results.

Let us mention that the components of the rate-of-strain tensor $[\boldsymbol{c}]$ in the (ρ, ϕ) coordinates are easily obtained if these coordinates are completed by an axial one, let say ζ, so that (ρ, ϕ, ζ) form a cylindrical system of coordinates (in our problem, ζ is perpendicular to the meridional plane); we show in appendix the equivalence of these expressions with the usual ones. In these coordinates, the rate-of-strain tensor components are

$$c_{\rho\rho} = c_{\phi\phi} = 2 \left(\frac{1}{\rho} \frac{\partial^2 \psi}{\partial \rho \partial \phi} - \frac{1}{\rho^2} \frac{\partial \psi}{\partial \phi} \right), \quad c_{\rho\phi} = \frac{\partial^2 \psi}{\partial \rho^2} - \frac{1}{\rho} \frac{\partial \psi}{\partial \rho} - \frac{1}{\rho^2} \frac{\partial^2 \psi}{\partial \phi^2},$$

$$c_{\rho\zeta} = \frac{\partial u}{\partial \rho}, \quad c_{\phi\zeta} = \frac{1}{\rho} \frac{\partial u}{\partial \phi},$$

and the volumic dissipation reads

$$D = 2(|c_{\rho\rho}|^2 + |c_{\rho\zeta}|^2 + |c_{\phi\zeta}|^2 + |c_{\rho\phi}|^2).$$

2.5. *Results*

For comparison with previous work, in all the numerical applications, we set the ratio of the inner radius to the outer one η to 0.35 which is the value of the Earth's liquid core.

M. Rieutord and L. Valdettaro

Tidal forcing, Ekman = 10^{-7}

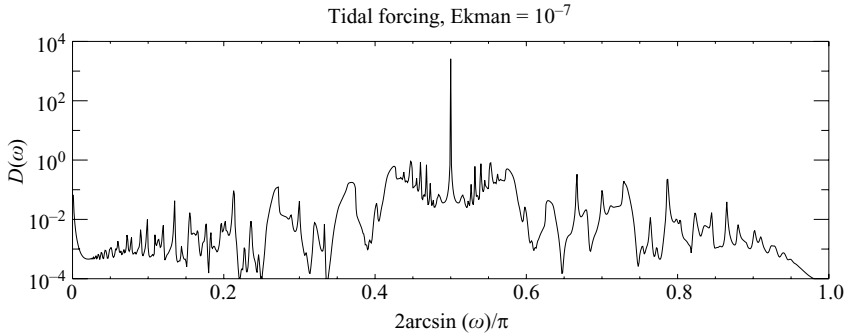
FIGURE 2. Scan of the dissipation as a function of the critical latitude angle at $E = 10^{-7}$. Resolution is $Nr = 180$, $N_\phi = 400$.

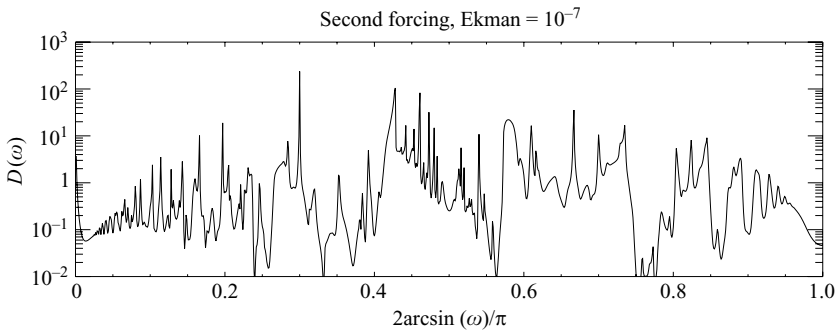Second forcing, Ekman = 10^{-7}

FIGURE 3. Same as in figure 2, but for the second forcing.

2.5.1. *Overall properties*

As shown by Witte & Savonije (1999*b*), during the evolution of the orbits, the tidal forcing frequency scans the whole inertial band and resonances there play a major part. Let us point out that in the text below, we shall understand the term 'resonance' as the local maximum (in frequency) of the viscous dissipation. This definition is appropriate for our problem but slightly different from the usual one which refers to the amplitude of the flow. Resonances are usually understood as the signature of the excitation of eigenmodes. As will be clear later, this classical view is not always appropriate here because of the ill-posed nature of the inviscid problem. Thus our wording 'resonance' should be understood in a rather loose way.

With the tidal forcing in mind, we simulate a scan of the inertial band. We represent the viscous dissipation as a function of the frequency, or, more appropriately, as a function of the critical latitude $\vartheta = \arcsin(\omega)$. As shown by figures 2 and 3, the curve $D(\omega)$ is very spiky and almost symmetric with respect to $\pi/4$. This underlying symmetry is a consequence of an invariance of Poincaré equation in two dimensions. Indeed, setting $E = 0$ in (2.1) and rewriting the equation for ψ, we find

$$\frac{\partial^2 \psi}{\partial s^2} - \left(\frac{1 - \omega^2}{\omega^2} \right) \frac{\partial^2 \psi}{\partial z^2} = F(s, z, \omega)$$

in the two-dimensional limit. If $F = 0$ we easily see that this equation is invariant with respect to the transformation $s \to z$, $z \to s$ and $\omega \to \sqrt{1 - \omega^2}$. Thus the place of

(a)

(b)

E_k

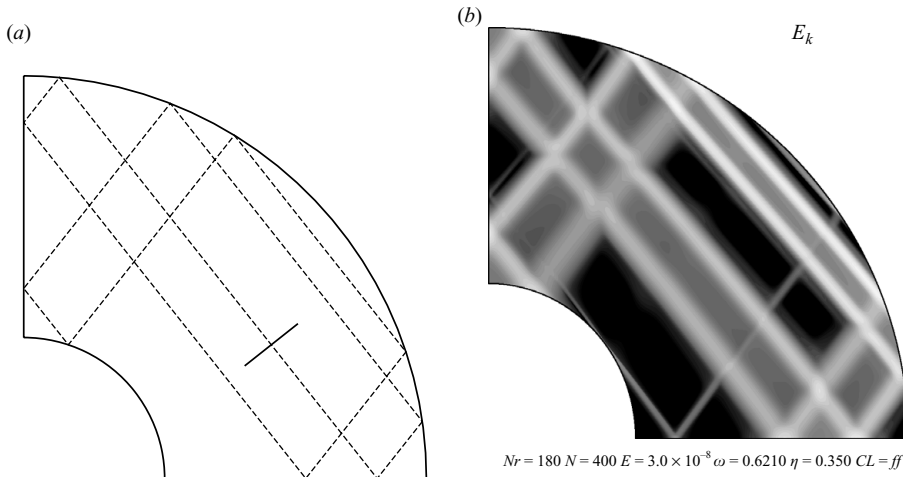$Nr = 180\ N = 400\ E = 3.0 \times 10^{-8}\ \omega = 0.6210\ \eta = 0.350\ CL = ff$

FIGURE 4. The attractor occupying the frequency band [0.60922, 0.62276]. Although prominent in the three-dimensional problem, this attractor cannot be excited by the natural tidal forcing; fortunately it can be studied with the second forcing. (a) The small segment indicates the place where the velocity profiles of figure 6 have been taken. (b) The kinetic energy distribution in a meridional plane for a numerical solution computed at $\omega = 0.621$ and $E = 3 \times 10^{-8}$.

resonant frequencies is indeed symmetric with respect to $\pi/4$, if the critical latitude is used as a variable. However, the final curves, which are shown in figures 2 and 3, partially lose their symmetry because the forcing does not verify the foregoing invariance as well as the viscous terms (the second forcing breaks more strongly this symmetry).

2.5.2. *Attractors and associated resonances*

To better understand the properties of the dissipation curves as shown in figures 2 and 3, we shall first concentrate on a given attractor, which is displayed in figure 4. This attractor may be found in the frequency range $[\omega_a, \omega_b]$ where $\omega_b = \sqrt{(5 - \sqrt{5 - 4\eta})/8}$ (ω_a has no analytic expression). In figure 5 we give a detailed view of the resonance associated with this attractor around its asymptotic frequency ω_b.

The remarkable property of these curves is the independence of dissipation from viscosity for frequencies far from the asymptotic frequency ω_1. This result perfectly illustrates the demonstration of Ogilvie (2005) who showed that dissipation by inertial modes associated with attractors with a finite Lyapunov exponent is actually independent of the Ekman number. This comes from the width of the associated shear layers, which scale like $E^{1/3}$. Figure 6 indeed confirms that velocity gradients inside a shear layer vary on a scale changing with the one-third power of the viscosity.

In Rieutord *et al.* (2002) however, it was shown that shear layers associated with freely decaying inertial modes, shaped by attractors, have a width scaling like $E^{1/4}$. This means that at resonances, dissipation resulting from the excitation of such singular modes diverges as $E^{-1/4}$ in the asymptotic limit of small Ekman numbers (see §2.5.4). Moreover, as shown by Rieutord *et al.* (2002), the frequency of these eigenmodes is of the form $\omega = \omega_0 + \omega_1 E^{1/2}$ for $E \ll 1$. We thus expect resonance widths to be of the order of $E^{1/2}$. Figure 5(b) perfectly illustrates these properties, showing that if scaled properly, resonance curves are independent of viscosity.
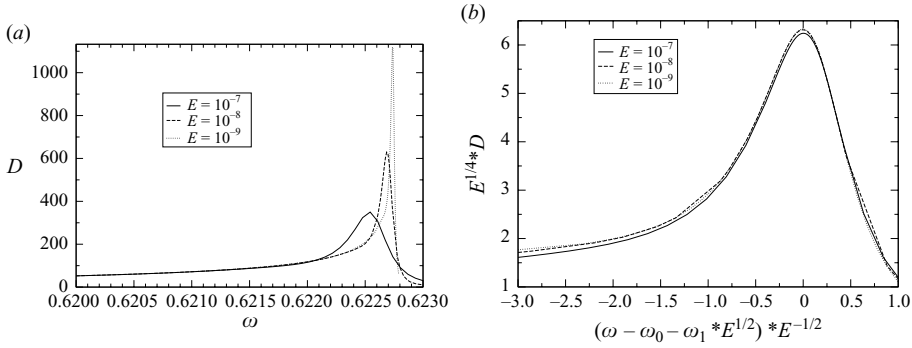
FIGURE 5. (*a*) Dissipation as a function of forcing frequency ω near the attractor of figure 4. Note that far from the resonance the dissipation tends to be independent of the Ekman number E. (*b*) For the same attractor, scaled resonance curves. Note that when scaled as indicated, dissipation curves no longer depend on viscosity. Here $\omega_0 = \omega_b$ is the upper bound of the frequency interval of the attractor.
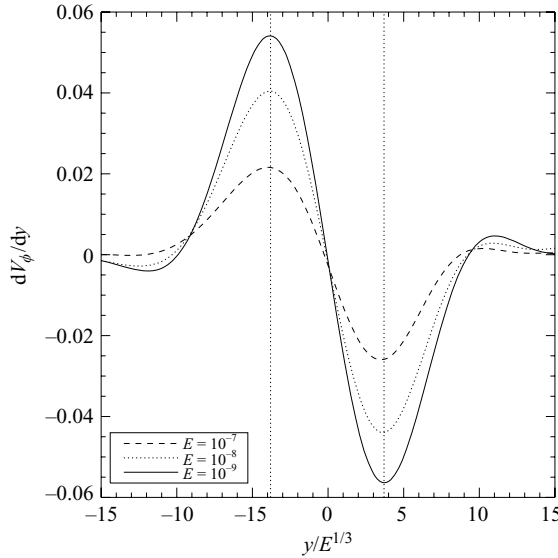

FIGURE 6. Profiles of the derivative $\mathrm{d}v_\phi/\mathrm{d}y$ along the straight thick line shown in figure 4(*a*) crossing a segment of the attractor at $\omega = 0.621$, $\eta = 0.35$. The abscissa is normalized by $E^{1/3}$: note that the location of the maxima of $\mathrm{d}v_\phi/\mathrm{d}y$ is nearly the same for the three profiles, showing that the width of the layer scales with $E^{1/3}$.

2.5.3. *Resonances associated with periodic orbits*

The foregoing resonances are not the strongest, however. Indeed, we have shown in Rieutord *et al.* (2001), that there exist a finite number of frequencies of the spectrum which are associated with strictly periodic orbits of the characteristics. These frequencies are $\omega_{p,q} = \sin(p\pi/2q)$ where p and q are integers; they are such that the angle between characteristics and the rotation axis is a rational fraction of π. Not all the rationals are allowed however, because characteristics must propagate periodically inside or outside the 'shadow' of the inner shell (see Rieutord *et al.* 2001). This condition imposes that $\eta \leqslant \omega \leqslant \sqrt{1-\eta^2}$ for the simplest periodic orbits (it is

(a)

(b)

E_k

$Nr = 50$ $N = 100$ $E = 1.0 \times 10^{-7}$
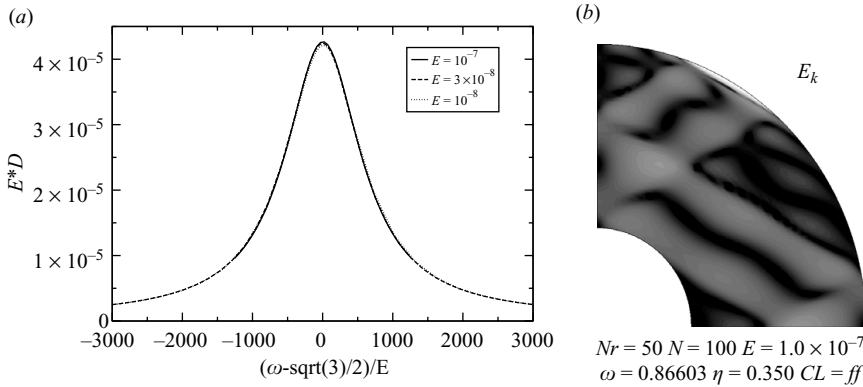$\omega = 0.86603$ $\eta = 0.350$ $CL = ff$

FIGURE 7. (a) Rescaled dissipation as a function of the forcing frequency, also rescaled, near the periodic orbits with $\theta_{cl} = \pi/3$ or $\omega = \sqrt{3}/2$. (b) The kinetic energy distribution of the corresponding forced flow at $E = 10^{-7}$.

more restrictive for more complex orbits). In the case chosen here, namely $\eta = 0.35$, the allowed periodic orbits are associated with the three angles: $\pi/6$, $\pi/4$ and $\pi/3$. For the associated frequencies the trajectories of characteristics are strictly periodic, thus no shear layer is generated (the mapping has no focusing power). This situation is illustrated in figure 7. As shown, no small scale comes in, and the dissipation diverges as E^{-1} when $E \to 0$, while the width of the resonances diminishes as E. Inspecting the spectral content of the flow, we note that the critical latitude contributes to some parts of the flow but at such a low level (less than 10^{-4}) that it does not influence the resonance.

This feature of the spectrum may be understood as follows. Maas & Lam (1995) showed that the two-dimensional semi-elliptic basin owns a denumerable set of regular eigenmodes. These eigenmodes are associated with periodic orbits of characteristics. They also showed that the eigenfrequencies are infinitely degenerate. This is because of the ill-posed nature of the eigenvalue problem: for each eigenvalue, the eigenmode is defined by an arbitrary function which is given on the so-called fundamental intervals of the boundary (see Maas & Lam 1995 for details). In the case of our fluid domain, the presence of an inner core removes almost all the periodic orbits, letting only a finite number of them, depending on the size of the core. However, for each of these frequencies which are of the form $\sin(p\pi/q)$ (see the first paragraph of §2.5.3), the associated eigenfunctions are still infinitely degenerate since they are specified by an arbitrary function. We illustrate this property by computing the first eigenmodes associated with these orbits (see table 1 and figure 8).

The response of the fluid to a time-periodic forcing near these frequencies thus results essentially from the superposition of these eigenmodes according to their projection on the exciting body force. As the tidal forcing is on the large scale, the responding flow is essentially on the large scales.

2.5.4. *Dissipation at resonances*

The foregoing resonances, either associated with attractors (§2.5.2) or with periodic orbits (§2.5.3), may be described by a simple model of a resonating eigenmode. Although much simplified, this model is useful to understand the origin of the scaling laws verified by the viscous dissipation.

	$\vartheta = \pi/6$		$\vartheta = \pi/4$	$\vartheta = \pi/3$	
	ω_2	τ_1	τ_1	ω_2	τ_1
Mode 1	1.6×10^8	-2.8×10^3	-1.05×10^2	-2×10^8	-2.8×10^3
Mode 2	5.8×10^9	-1.5×10^4	-4.32×10^2	-8×10^9	-1.5×10^4
Mode 3	3.8×10^{10}	-3.8×10^4	-9.64×10^2	-6×10^{10}	-3.7×10^4

TABLE 1. Eigenvalues of the first modes associated with periodic orbits of the torus and verifying the same symmetry as the forcing (2.3). Each eigenvalue is written $\lambda = \mathrm{i}\sin\vartheta + \mathrm{i}\omega_2 E^2 + \tau_1 E$, as expected for regular modes with stress-free boundary conditions when $\omega_1 = 0$ (the reason for this vanishing term is not clear). The ω_2 term for the $\pi/4$ modes could not be evaluated because of round-off errors. The coefficients τ_1 and ω_2 have been evaluated numerically using values of E around 10^{-7}.
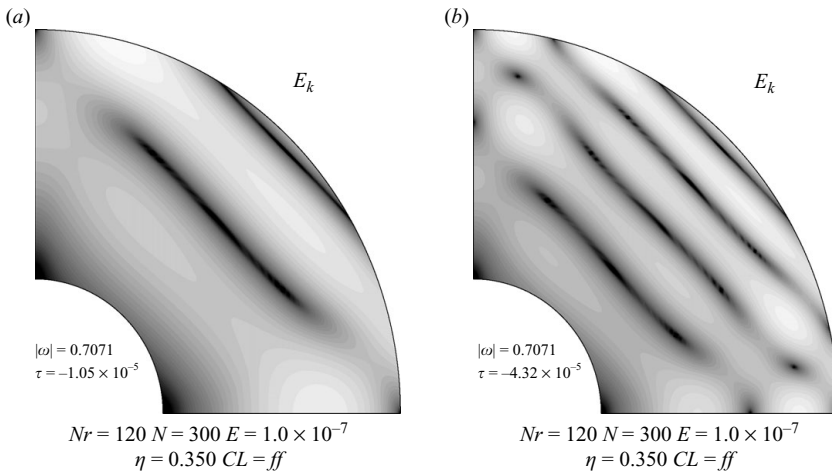

FIGURE 8. Kinetic energy distribution of the two first modes associated with the $\vartheta = \pi/4$ periodic orbit given in table 1.

Let $\mathscr{L}$ be the linear operator governing the forced flow; we write

$$\mathrm{i}\omega\boldsymbol{u} = \mathscr{L}(\boldsymbol{u}) + \boldsymbol{f}, \qquad (2.5)$$

where ω is the frequency of the forcing. Let $\{\boldsymbol{u}_n\}_{n\in\mathbb{N}}$ be a set of eigenfunctions of $\mathscr{L}$ verifying the same boundary conditions as $\boldsymbol{u}$. Hence

$$\lambda_n \boldsymbol{u}_n = \mathscr{L}(\boldsymbol{u}_n),$$

where $\lambda_n = \mathrm{i}\omega_n + \tau_n$ is the associated eigenvalue. We assume that the $\{\boldsymbol{u}_n\}_{n\in\mathbb{N}}$ form a complete orthogonal basis. As far as modes associated with an attractor are concerned, we have shown in Rieutord *et al.* (2002), that they may be described by a Hermite function. They thus form a complete basis for the one-dimensional functions defined along a line orthogonal to the attractor. Thus we may write

$$\boldsymbol{u} = \sum_n a_n \boldsymbol{u}_n, \quad \boldsymbol{f} = \sum_n f_n \boldsymbol{u}_n.$$

Here, we assumed that $\boldsymbol{f}$ belongs to the same function space as $\boldsymbol{u}$. From (2.5), we easily find that $a_n = f_n/(\mathrm{i}\omega - \lambda_n)$ so that

$$\boldsymbol{u} = \sum_n \frac{f_n \boldsymbol{u}_n}{\mathrm{i}\omega - \lambda_n}. \tag{2.6}$$

Now assuming that a single eigenmode dominates the series, we simplify (2.6) as

$$\boldsymbol{u} \simeq \frac{f_n \boldsymbol{u}_n}{\mathrm{i}\omega - \lambda_n}.$$

The dissipation rate can now be evaluated from (2.4). The width of the shear layers is assumed to scale like E^α. The volume that contains the shear layers also scales like E^α and the gradients of the eigenmode $\boldsymbol{u}_n$ scale like $E^{-\alpha}$. We get

$$D = \frac{E}{2} \int_{(V)} |c|^2 \,\mathrm{d}V \sim \frac{E^{1-\alpha}}{(\omega - \omega_n)^2 + \tau_n^2}. \tag{2.7}$$

Assuming that the complex eigenfrequency of the excited mode expresses as $\lambda_n = \mathrm{i}\omega_n + \lambda_1 E^\beta$, we find that

$$D \sim E^{1-\alpha-2\beta}$$

at the resonance. For resonances associated with attractors with vanishing Lyapunov exponents, the solutions of Rieutord *et al.* (2002) give $\alpha = 1/4$, $\beta = 1/2$ and thus $D \sim E^{-1/4}$ as observed numerically. For the sharp resonances associated with the periodic orbits of §2.5.3, no small scales comes in so that $\alpha = 0$. The damping rate of a mode with a typical scale independent of viscosity is proportional to E; thus $\beta = 1$ and we get $D \sim E^{-1}$ as also observed.

Although not fully rigorous, this short analysis shows that the observed resonances of the two-dimensional model behave in a standard way.

2.6. *The critical latitude singularity*

Before ending this section we wish to discuss shortly the role played by the critical latitude singularity. We recall that this singularity comes from the 'oblique nature' of the boundary conditions to be used with the Poincaré equation (see Rieutord *et al.* 2001). It leads to a singularity of the solutions but weaker than the one associated with the attractors. When the problem takes into account the fluid's viscosity, this singularity manifests itself as a broadening of the Ekman layer, which thickens from the usual $E^{1/2}$ scale to the $E^{2/5}$ scale, on a latitudinal extension that is $O(E^{1/5})$ (Roberts & Stewartson 1963). As illustrated in figure 4 this singularity generates its own network of shear layers thus adding some dissipation to the one of the attractor. However, the contribution of this singularity is much smaller than the one of the attractor. We also observe that if the frequency of the forcing is not such that the attractor has a branch grazing at the critical latitude, the amplitude of the flow in this region vanishes with a vanishing Ekman number.

2.7. *Summarizing the two-dimensional case*

The preceding results show that the dissipation associated with periodically forced shear layers may vary very strongly as a function of the frequency of the forcing. At a generic frequency, we find that the dissipation is independent of the viscosity and thus confirm the analysis of Ogilvie (2005). However, the inertial frequency band contains also infinitely many frequencies (at accumulation points) where attractors are weaker (their Lyapunov exponent vanishes and the convergence of characteristics

is algebraic instead of exponential). At these points the dissipation strongly depends on viscosity, namely as $E^{-1/4}$. Finally, we also exhibited resonances that are associated with the few allowed periodic orbits of characteristics. These resonances are those of the regular modes which remain of the dense set of modes of the $\eta = 0$ torus (see Maas & Lam 1995). As these periodic orbits, there is only a finite number of such resonances for a given set-up with $\eta \neq 0$.

We now examine the three-dimensional case so as to determine which of these properties remain in this more realistic case.

3. Resonances in the spherical shell

3.1. *Numerics*

Turning to the spherical shell problem, we now solve (1.1) in spherical geometry. We discretize the unknowns and the equations using an expansion of the fields on the spherical harmonics $Y_\ell^m(\theta, \varphi)$ for the horizontal part and using the Chebyshev polynomials on the Gauss–Lobatto collocations nodes for the radial part. Details may be found in Rieutord & Valdettaro (1997). We just recall here that the velocity field is expanded as

$$\boldsymbol{u} = \sum_{l=0}^{+\infty} \sum_{m=-l}^{+l} u_m^\ell(r)\boldsymbol{R}_\ell^m + v_m^\ell(r)\boldsymbol{S}_\ell^m + w_m^\ell(r)\boldsymbol{T}_\ell^m$$

with

$$\boldsymbol{R}_\ell^m = Y_\ell^m(\theta, \varphi)\boldsymbol{e}_r, \quad \boldsymbol{S}_\ell^m = \nabla Y_\ell^m, \quad \boldsymbol{T}_\ell^m = \nabla \times \boldsymbol{R}_\ell^m,$$

where gradients are taken on the unit sphere. Using the same expansion for the body force (1.2), we find

$$\boldsymbol{f} = \mathscr{A} r^2 \left(-\mathrm{i}\omega \boldsymbol{R}_2^0 + \frac{1}{\sqrt{15}}\boldsymbol{T}_1^0 - \frac{12}{\sqrt{35}}\boldsymbol{T}_3^0 \right).$$

Following Rieutord (1987), we derive the equations for the radial functions $u_m^\ell(r)$ and $w_m^\ell(r)$ from the equations of vorticity and continuity. They read

$$\left.\begin{aligned}
E\Delta_\ell w^\ell - \mathrm{i}\omega w^\ell &= -A_\ell r^{\ell-1}\frac{\partial}{\partial r}\left(\frac{u^{\ell-1}}{r^{\ell-2}}\right) \\
&\quad - A_{\ell+1} r^{-\ell-2}\frac{\partial}{\partial r}(r^{\ell+3}u^{\ell+1}) - r^2\left(\frac{\delta_{\ell,1}}{\sqrt{3}} - \frac{12}{\sqrt{7}}\delta_{\ell,3}\right), \\
E\Delta_\ell\Delta_\ell(ru^\ell) - \mathrm{i}\omega\Delta_\ell(ru^\ell) &= B_\ell r^{\ell-1}\frac{\partial}{\partial r}\left(\frac{w^{\ell-1}}{r^{\ell-1}}\right) \\
&\quad + B_{\ell+1} r^{-\ell-2}\frac{\partial}{\partial r}(r^{\ell+2}w^{\ell+1}) - \mathrm{i}\omega 6\sqrt{5}r\delta_{\ell,2},
\end{aligned}\right\} \tag{3.1}$$

where axisymmetry has been assumed. We have used

$$A_\ell = \frac{1}{\ell\sqrt{4\ell^2-1}}, \quad B_\ell = \ell^2(\ell^2-1)A_\ell, \quad \Delta_\ell = \frac{1}{r}\frac{d^2}{dr^2}r - \frac{\ell(\ell+1)}{r^2}.$$

The set of equations (3.1) is completed by stress-free boundary conditions, which read

$$u_m^\ell = \frac{\partial^2 r u_m^\ell}{\partial r^2} = \frac{\partial}{\partial r}\left(\frac{w_m^\ell}{r}\right) = 0$$
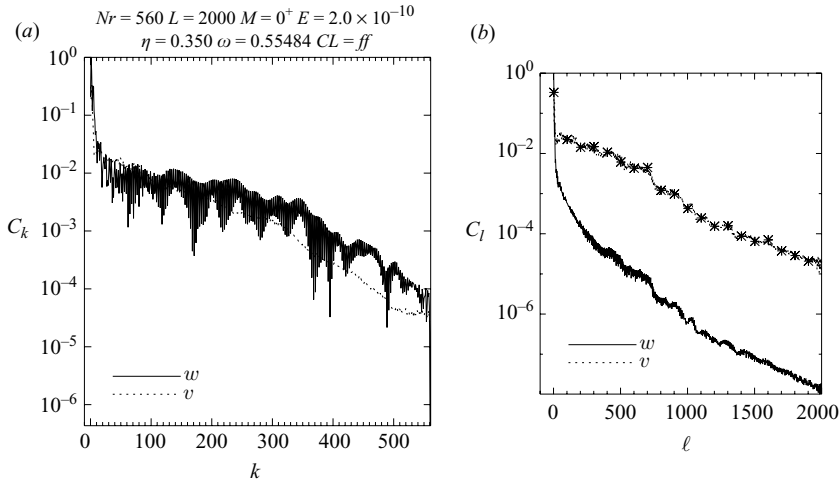
for the radial functions taken at $r = \eta$ or $r = 1$.

FIGURE 9. Spectral content of the solution shown in figure 14(*c*). (*a*) Maximum Chebyshev spectrum of the velocity field: for a given order of the Chebyshev coefficient we plot the maximum absolute value of the coefficient obtained over all the spherical harmonic components. (*b*) The maximum spherical harmonic spectrum of the velocity field: for each spherical harmonic order ℓ we plot the largest absolute value of all the Chebyshev coefficients; w refers to w^ℓ while v refers to ru^ℓ (see also Rieutord & Valdettaro 1997).

In figure 9, we give an example of the spectral content of the forced flow shown in figure 14(*c*), for $E = 2 \times 10^{-10}$. The spectra show that the truncation error of the solutions are $O(10^{-4})$, while we estimated the round-off error (with double precision arithmetics) to a lower value, in this case (see Valdettaro *et al.* 2007, for a more thorough discussion of these error matters).

3.2. *Overall view of the resonance spectrum*

As for the two-dimensional case, we first scan the whole inertial band, computing the viscous dissipation. The result is plotted in figure 10. There we note that the response curve is very spiky as in the two-dimensional case, revealing very strong variations (six orders of magnitude at $E = 10^{-8}$). We plotted the quantity $\omega^2 D(\omega)$ to remove the $1/\omega^2$ divergence at low frequencies, since in this range, the flow is dominated by the velocity field $\boldsymbol{u} = Ar^2 \sin\theta/\omega\boldsymbol{e}_\phi$. The broad shape of the curve does not show a marked symmetry with respect to $\vartheta = \pi/4$ unlike its two-dimensional counterpart (figure 2). This is expected since the curvature terms of the three-dimensional operators contribute to break this symmetry. Another striking difference is the absence of resonances at the three frequencies corresponding to strictly periodic orbits of characteristics, namely $\vartheta = \pi/6, \pi/4, \pi/3$. On the contrary, there is an antiresonance phenomenon.

Before discussing in more details some specific features of this curve, let us focus on figure 11. Here, following the idea of Ogilvie (2009), we have plotted the dissipation curve when a frictional force $-\gamma\boldsymbol{u}$ replaces the viscous force $E\Delta\boldsymbol{u}$. As shown by figure 11, the two curves are very similar, demonstrating that the fluid response is mainly governed by the underlying Poincaré operator (i.e. the operator governing the inviscid problem). The meaning of this similarity and the relation with the Poincaré operator may be enlighted when using this simple frictional force. In this case the
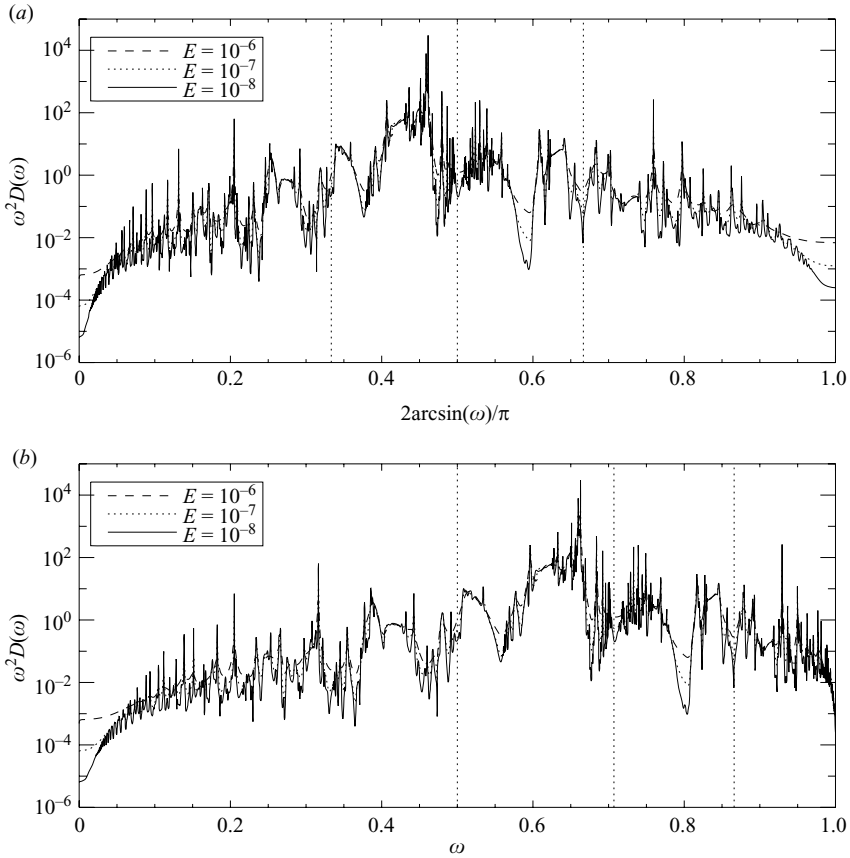
FIGURE 10. Scan of the whole inertial band for the viscous dissipation in a spherical shell. Vertical dotted lines mark the frequencies allowing strictly periodic orbits of characteristics $\vartheta = \pi/6, \pi/4, \pi/3$.

flow verifies

$$
\left.
\begin{aligned}
(\mathrm{i}\omega + \gamma)\boldsymbol{u} + \boldsymbol{e}_z \times \boldsymbol{u} &= -\nabla p + \boldsymbol{f}, \\
\nabla \cdot \boldsymbol{u} &= 0.
\end{aligned}
\right\}
\tag{3.2}
$$

Setting $\lambda = \mathrm{i}\omega + \gamma$, this problem, which is completed by the boundary condition $\boldsymbol{u} \cdot \boldsymbol{n} = 0$, may be symbolically written as

$$
\lambda \begin{pmatrix} \mathrm{Id} & 0 \\ 0 & 0 \\ 0 & 0 \end{pmatrix} \begin{pmatrix} \boldsymbol{u} \\ p \end{pmatrix} = \begin{pmatrix} -\boldsymbol{e}_z \times & -\nabla \\ \nabla \cdot & 0 \\ \boldsymbol{n} \cdot & 0 \end{pmatrix} \begin{pmatrix} \boldsymbol{u} \\ p \end{pmatrix} + \begin{pmatrix} \boldsymbol{f} \\ 0 \\ 0 \end{pmatrix}
$$

or

$$
(\lambda J - \mathscr{L}_P)\, \boldsymbol{X} = \boldsymbol{X}_f, \quad \boldsymbol{X} = \begin{pmatrix} \boldsymbol{u} \\ p \end{pmatrix}, \quad \boldsymbol{X}_f = \begin{pmatrix} \boldsymbol{f} \\ 0 \\ 0 \end{pmatrix}, \quad J = \begin{pmatrix} \mathrm{Id} & 0 \\ 0 & 0 \\ 0 & 0 \end{pmatrix}.
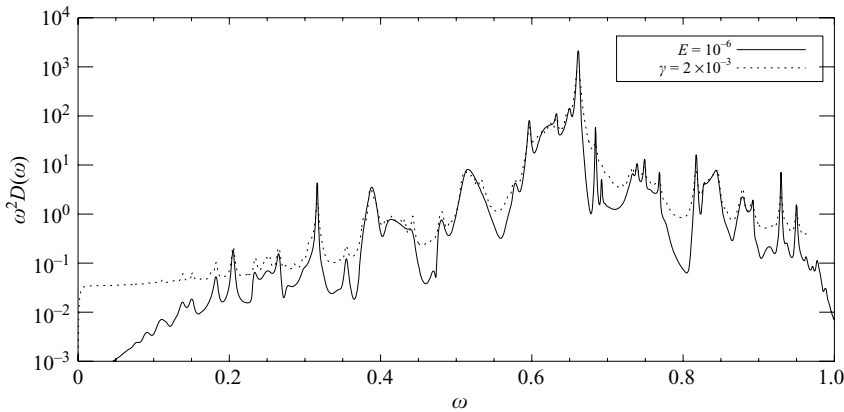$$

FIGURE 11. Scan of the whole inertial band for the dissipation using the viscous force (solid line) or the friction force (dotted line). Note the similarity of the curves.

Here, $X = {}^t(\boldsymbol{u}, p)$ and $\mathscr{L}_P$ symbolizes the Poincaré operator. Formally, the solution of the velocity field may be expressed as

$$\boldsymbol{u} = (\lambda J - \mathscr{L}_P)^{-1} \boldsymbol{f},$$

where $(\lambda J - \mathscr{L}_P)^{-1}$ is a kind of resolvent of the Poincaré operator, restricted to a vector field, since the operator J is 'close' to the identity. The dissipation associated with the flow is proportional to the norm of $\boldsymbol{u}$; indeed, it is

$$D = \gamma \int_{(V)} |\boldsymbol{u}|^2 \, \mathrm{d}V.$$

Hence, using a restriction of the norm of X to the velocity field, we may write the dissipation as

$$D = \|(\lambda J - \mathscr{L}_P)^{-1} \boldsymbol{f}\|^2.$$

Now, let us consider the ϵ-pseudospectrum of the Poincaré operator. This quantity is indeed very appropriate to deal with a non-normal operator such as the Poincaré one (see Trefethen & Embree 2005). It is defined as the set of complex numbers λ such that

$$\|(\lambda J - \mathscr{L}_P)^{-1}\| > 1/\epsilon,$$

where we recall that the norm of a bounded linear operator L is the number

$$\max_{\text{over } X} \left(\frac{\|L X\|}{\|X\|} \right).$$

We therefore see that all the regions of the frequency axis where $D > \gamma/\epsilon^2$ belong to the ϵ-pseudospectrum of the Poincaré operator. Indeed, if $D > \gamma/\epsilon^2$ then

$$1/\epsilon < \|(\lambda J - \mathscr{L}_P)^{-1} \boldsymbol{f}\| \leqslant \|(\lambda J - \mathscr{L}_P)^{-1}\|,$$

where we assumed that $\|\boldsymbol{f}\| = 1$.

Thus, the dissipation curve obtained with the frictional force gives a partial (one-dimensional) view of the ϵ-pseudospectrum of the Poincaré operator; computing the curve for many γ would give a view of the two-dimensional subsets of the complex plane, which belong to this pseudospectrum.

Now, the similarity of the two dissipation curves associated with the two damping forces, comes from the nature of the solutions. When these are in the form of a well defined attractor, the width of the shear layers is a small scale that singles out so that $E\Delta\boldsymbol{u} \sim -Ek^2\boldsymbol{u}$, where $k \sim E^{-1/3}$.

To conclude this point, we see that the solution of the forced problem shows another side of the Poincaré operator, namely its pseudospectrum, and this quantity is independent of both the forcing and the frictional force. The peaks of the dissipation curves offer a partial (one-dimensional) view of this quantity.

3.3. *Antiresonances at periodic orbits of characteristics*

We designate by antiresonances of the dissipation curve, the frequencies for which the dissipation vanishes with the Ekman number.

We consider the three strictly periodic orbits authorized in the shell with $\eta = 0.35$, namely those orbits for which characteristics remain either inside or outside the shadow of the inner core (see Rieutord *et al.* 2001). These are associated with $\vartheta = \pi/6, \pi/4, \pi/3$. We plot in figure 12 the dissipation for these three values and note that it decreases following quite closely the law $D \propto E^{2/5}$. Such a scaling is obviously reminiscent of the critical latitude boundary layer. Actually, as shown by figure 12(*b*), the fluid's oscillation is confined along the characteristics emitted by the critical latitude boundary layer.

One may retrieve the scaling of dissipation if we note that the volume of the boundary layer surrounding the critical latitude singularity is $O(E^{1/5+2/5})$ and that the velocity field scales as $E^{-1/5}$. This scaling appears if we observe that the singular inviscid field has a finite normal velocity at the boundary and an infinite tangential velocity (see Rieutord *et al.* 2001). Assuming that u_r is of order unity (as the forcing), boundary layers relations imply that the tangential velocity scales as $E^{-1/5}$. Using the second expression of the dissipation, $D = \int_{(V)} Re(\boldsymbol{u}^* \cdot \boldsymbol{f}) \, dV$, we recover the scaling law that we observe numerically. We note that this regularized singularity, propagates along the (periodic path of) characteristics, but without any focusing, the resulting shear layer widens slowly as we move away from the critical latitude of the inner bounding sphere.

3.4. *Dissipation in the frequency bands with strong attractors*

One of the main results established in two dimensions is that a forced flow oscillating at the frequency of an attractor dissipates energy independently of viscosity, provided it is low enough. As shown in figure 13, which gives a zoom on the dissipation curve, we clearly see a region of the spectrum (below $\omega = 0.624$) where the dissipation is independent of the Ekman number. The curve in figure 12 (diamonds) confirms this convergence to a finite dissipation as viscosity vanishes.

There is however a surprise in this case. If we look at the Lyapunov exponent in the same frequency band we note that something should happen at the frequency ω_0 where this exponent vanishes. According to the results of Rieutord *et al.* (2001), we should expect a resonance, as in two dimensions. No such resonance occurs, and this is independent of the symmetry of the forcing. Inspection of the associated flow (see figure 13*c*) shows that the attractor is not excited. Rather, the critical latitude singularity excites a shear layer, which propagates towards the attractor. This is all the more surprising that in this frequency band there are many eigenmodes well centred on the attractor path (an example may be found in Rieutord *et al.* 2001).

This situation is not unique: it is also the case when we consider the simple attractor occupying the frequency band [0.529, 0.555]. As shown in figure 14, no resonance occurs there. Actually, if we compare the least damped eigenmode associated with
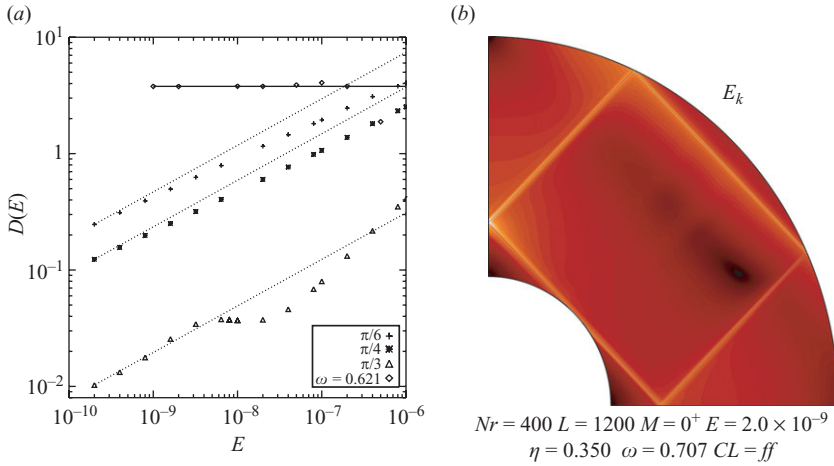
FIGURE 12. (*a*) Dissipation as a function of the Ekman number for four given frequencies. 'Diamonds': $|D(E) - D(E = 10^{-6})|$ for a forcing frequency exciting the attractor shown in figures 4 and 13 at $\omega = 0.621$. 'Pluses', 'stars' and 'triangles' show the dissipation at frequencies respectively: $\sin(\pi/6)$, $\sin(\pi/4)$ and $\sin(\pi/3)$; the dotted straight lines emphasize the power law $D(E) \propto E^{2/5}$. (*b*) The kinetic energy distribution for a forcing at $\omega = \sin(\pi/4)$ and $E = 2 \times 10^{-9}$.
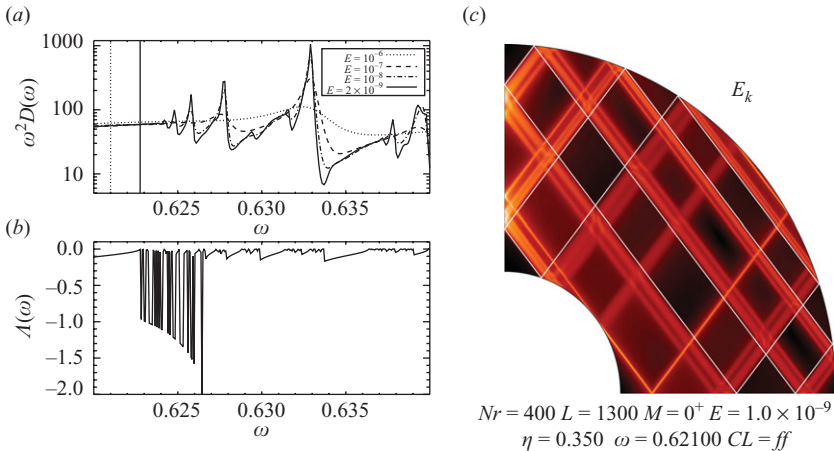

FIGURE 13. (*a*) Zoom of the dissipation in the spherical shell for $\omega \in [0.62, 0.64]$. (*b*) The associated Lyapunov exponents in the same frequency range. (*c*) The kinetic energy of the forced flow at $\omega = 0.621$ viewed in a meridional plane. The white line marks the path of the attractor.

this attractor and the forced flow of the same frequency, which are shown in the same figure, we clearly see that the attractor is not excited. There too, we see that the shear layer emitted by the critical latitude is strongly excited. It propagates towards the attractor. The dissipation curves computed at various Ekman numbers shows that for these values of E, no asymptotic regime is reached. Actually, a calculation for a specific frequency shows that an asymptotic regime exists but at a very low Ekman number ($\lesssim 10^{-12}$). We also note that the Ekman number below which the viscous dissipation is constant depends on the 'distance' between the attractor and the characteristics emitted at the critical latitude. We observe that at $\omega = 0.542$ the
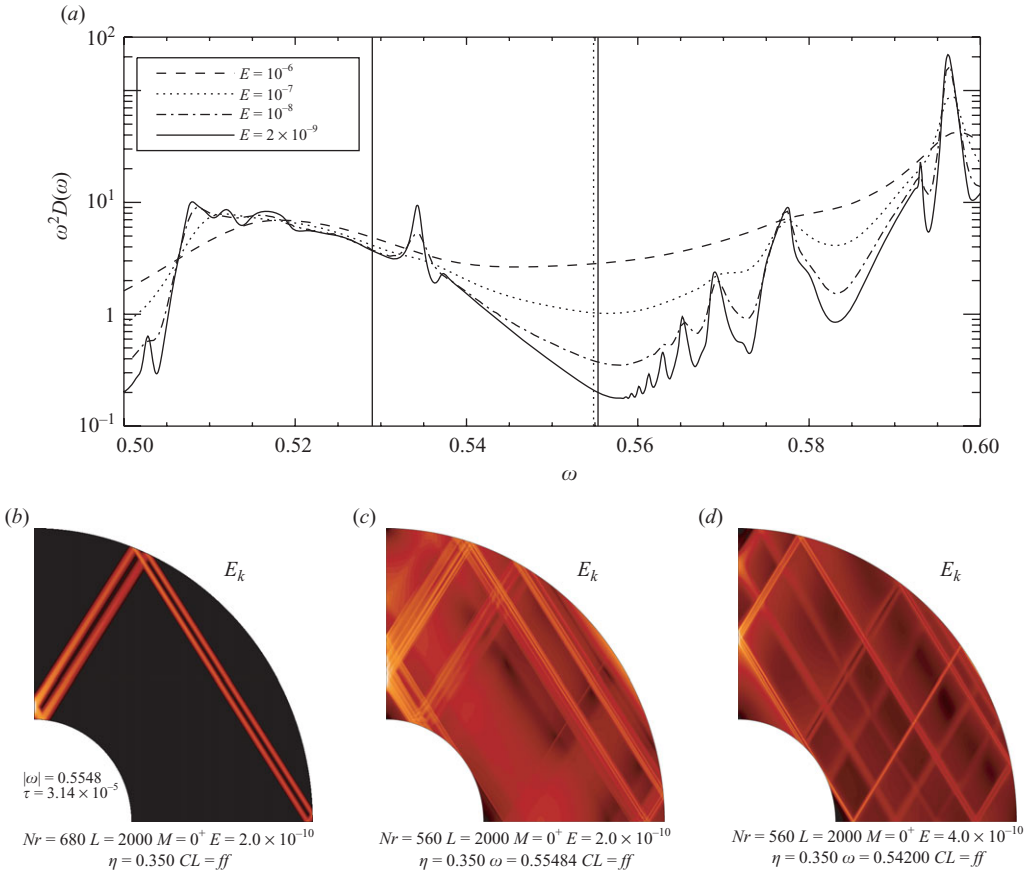
FIGURE 14. (*a*) Zoom of the dissipation curve for various Ekman numbers for $\omega \in [0.5, 0.6]$. The two vertical solid lines delineate the frequency range of the attractor shown by the eigenmode below. The dotted vertical line shows the frequency of the least damped eigenmode. (*b*) The kinetic energy distribution in a meridional plane of the least damped eigenmode ($\omega = 0.554838$) associated with the attractor governing this frequency range. (*c*) The amplitude of the forced flow at the frequency of the eigenmode. (*d*) The frequency of the forcing is now $\omega = 0.542$ so that the attractor is closer to the critical latitude. Note that a second attractor is now visible and excited by the southern branch of the shear layer emitted at the critical latitude.

asymptotic regime is almost reached; in this case, the attractor is much stronger and closer to the critical latitude (as confirmed by figure 14).

Back to the $\omega = 0.621$ case, we note that all dissipation curves at some frequencies above $\omega_0 = 0.622759$ (which is the upper limit of the attractor living at $\omega \leqslant \omega_0$), seem to have converged to a limit. We think that the asymptotic limit has not actually been reached there, and that undulations of the dissipation curve will appear, as they do at higher frequencies, in response to the rapid variations of the Lyapunov exponent.

To conclude this point, the foregoing examples show that the asymptotic regime, where dissipation is independent of viscosity, is reached when the Ekman number is low enough so that the shear layer emitted at the critical latitude on the inner boundary is 'feeding' an attractor. In this case the widening and softening of the shear layer, due to viscous diffusion, is stopped. The shear layers are then in a regime similar to what has been described by Ogilvie (2005) in two dimensions.
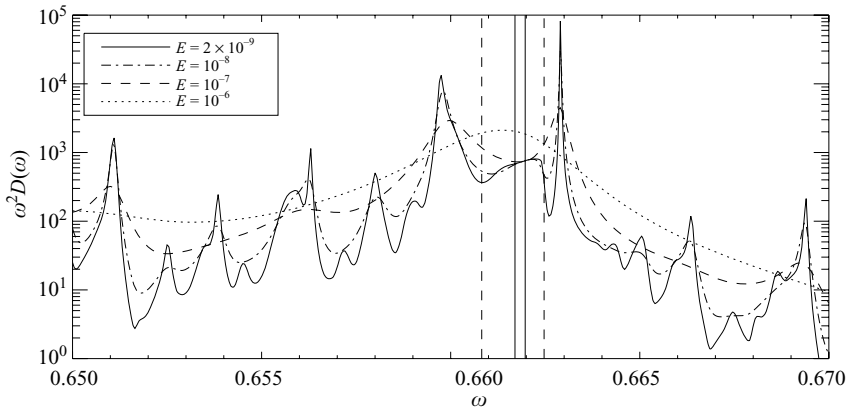
FIGURE 15. Zoom of the dissipation in the spherical shell in a given frequency range; the four vertical straight lines show the range of existence of two short-period attractors.

3.5. *Resonances*

The two-dimensional case gave a nice illustration of resonances which correspond to frequencies where the Lyapunov exponent vanishes. The foregoing discussion has shown that the three-dimensional situation is not so simple. Actually, we could not identify a single resonance that matches the frequency corresponding to the vanishing Lyapunov exponent of a well-determined attractor.

Nonetheless, dissipation curves show many peaks indicating some privileged frequencies. The formation of these peaks as viscosity decreases is not quite standard. Indeed, if we compare the dissipation curves in the interval [0.5, 0.6] (figure 14) and the one in the interval [0.65, 0.67] (figure 15), there is a common feature. It is the fact that 'resonant peaks' are more and more numerous as the viscosity decreases (as expected); however, they do not seem to appear because the resonances are more and more vigorous (it is only marginally the case), but because the neighbouring frequencies resonate less and less. Hence, it seems to be that many peaks are not true resonances, but small intervals of frequencies where the dissipation is independent of the viscosity provided it is low enough. The series of peaks for $\omega \in [0.56, 0.58]$ is quite illustrative of this phenomenon.

However, there are also some peaks which do behave like true resonances, i.e. their amplitude steadily increases as the Ekman number decreases. This is, for instance, the case of the two major peaks of the spectrum, lying at $\omega_1 = 0.6598$ and $\omega_2 = 0.6629$. These resonances correspond to the least damped axisymmetric inertial modes that we actually studied in Rieutord & Valdettaro (1997). We therefore extended this previous study to lower Ekman numbers. In figure 16, we focus our attention to the first mode, which seems to follow some asymptotic regime (as shown, the damping rate of the second mode is clearly not a power law). Figure 16 shows that the dissipation, there, grows like $E^{-1/3}$ when $E \gtrsim 10^{-9}$, but like $E^{-1/2}$ if $E \lesssim 10^{-9}$. On the other hand, the width of the resonance narrows as $E^{2/3}$ when $E \lesssim 10^{-9}$; we note that the associated eigenmode has a damping rate decreasing as $E^{0.57}$. Applying the simplified model of §2.5.4 to this case, we recover the scaling law of the viscous dissipation at $E \gtrsim 10^{-9}$ if we assume that the critical latitude singularity emits a shear layer of width $E^{1/5}$, i.e. corresponding to the latitudinal extension of the perturbed Ekman layer on the inner sphere. Hence, dissipation should scale as like $E^{4/5-2\beta}$. Using $\beta = 0.57$ we find $D \sim E^{-0.34}$. A similar matching of the exponents can be obtained if the forced flow
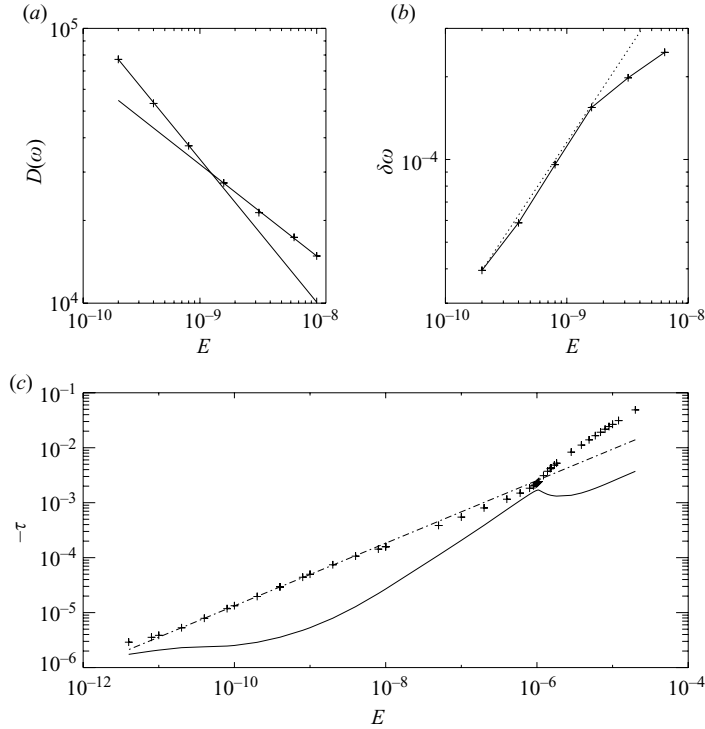
FIGURE 16. (*a*) The viscous dissipation at the resonance $\omega = 0.6598$ as a function of the Ekman number; the straight lines shows the power laws $E^{-1/3}$ and $E^{-1/2}$. (*b*) The solid line and pluses show the width $\delta\omega$ of the resonance compared to the power law $E^{2/3}$ (dotted line). (*c*) We show the damping rate τ of the two least damped eigenmodes at $\omega_1 = 0.6598$ (pluses) and $\omega_2 = 0.6629$ (solid line); the power law $E^{0.57}$ is shown by the dash-dotted straight line.

is confined to a neighbourhood of the critical latitude. The volume responding to the forcing is $O(E^{3/5})$ but the velocity gradients are $O(E^{-2/5})$, thus leading to the same power law for the dissipation. The simple model of §2.5.4 cannot be more precise, but it clearly underlines the crucial role played by the critical latitude. We refer the reader to the work of Kerswell (1995) for a detailed analysis of the boundary layers and shear layers in the vicinity of the critical latitude in the case of the spin-over mode (i.e the non-axisymmetric, $m = 1$ at $\omega = 0.5$, inertial mode).

Now, the power law change at $E \sim 10^{-9}$ may be understood with figure 17. In this figure we show an enlarged view of the resonance together with the Lyapunov exponents. It is clear that, as the Ekman number decreases, the resonance shifts to the frequency interval where this exponent is very small. We note that $E = 10^{-9}$ corresponds to the transition where the resonance leaves the frequency range occupied by a short-period attractor and enters the frequency interval where only long-period attractors exist, leading to a stronger resonance. The new $E^{-1/2}$ regime is likely not asymptotic as well: inspection of the Lyapunov curve shows that the size of the frequency intervals, where a definite Lyapunov exponent exists, is at least less than 10^{-8}. This means that an asymptotic regime may be reached at Ekman numbers less than 10^{-15} (assuming that the resonance keeps narrowing as $E^{2/3}$). Such numbers, even if theoretically reachable in stars or planets, are likely unrealistic because any small-scale turbulence would increase them by many orders of magnitude. Thus, the
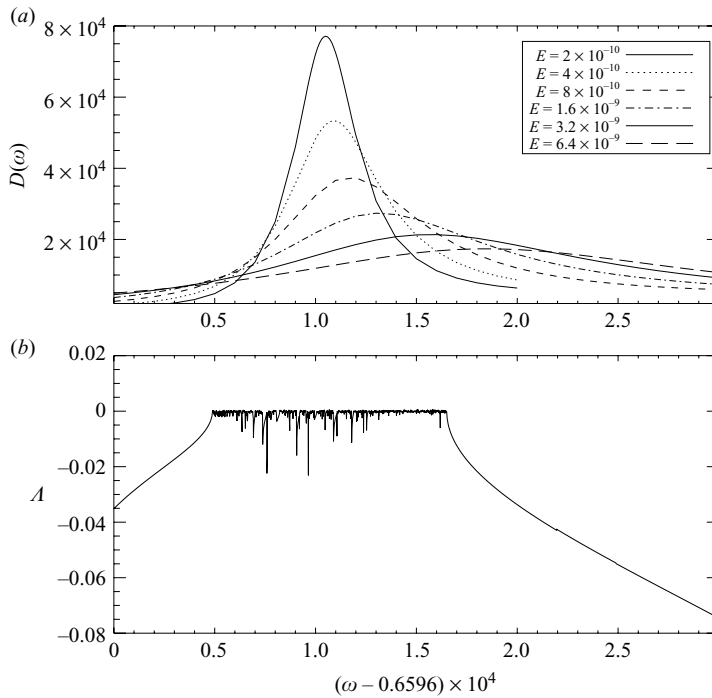
FIGURE 17. (a) The viscous dissipation at the resonance near $\omega = 0.6596$ as a function of the frequency for various Ekman numbers. (b) The corresponding Lyapunov exponents in the same frequency interval. Note the progressive move of the resonance peak towards the frequencies with small Lyapunov exponents.

intermediate regimes revealed by the $E^{-1/3}$ or $E^{-1/2}$ laws for the dissipation are likely to be more relevant to astrophysical or geophysical applications, but more investigations are needed to determine their origin.

3.6. *Influence of the size of the core*

A last question that is often raised is whether the size of the core, when it is small, influences notably the response curve that would be obtained if neglecting the core. From the foregoing results and the discussion of Rieutord *et al.* (2000), the answer to this question obviously depends on the Ekman number. It is indeed expected that for large viscosities, a small inner core is hardly seen by the fluid motion. To illustrate further this point we plot in figure 18, the dissipation curves for various sizes of the inner core together with the one of the full sphere. As shown, at a rather large Ekman number $E = 10^{-4}$ (unrealistic for planetary or stellar applications), the dissipation curve of the spherical shell notably differs from the full sphere case only when $\eta \geqslant 0.2$. On the other hand, with a more realistic value $E = 10^{-8}$, we note that a very small core $\eta = 0.05$ already amplifies the dissipation by an order of magnitude. One also observes that the frequencies of some resonances are quite similar. This likely comes from the polynomial nature of the full sphere solutions. Using a truncated solution in series of spherical harmonics, Rieutord (1991) showed that the frequency of one of the large-scale modes of the full sphere was shifted by an amount $O(\eta^5)$.

In fact, in the inviscid case, the presence of a small core, although fully perturbating the eigenvalue spectrum of the Poincaré operator, likely has a less drastic influence on the pseudospectrum, which we partially view through the dissipation curve.
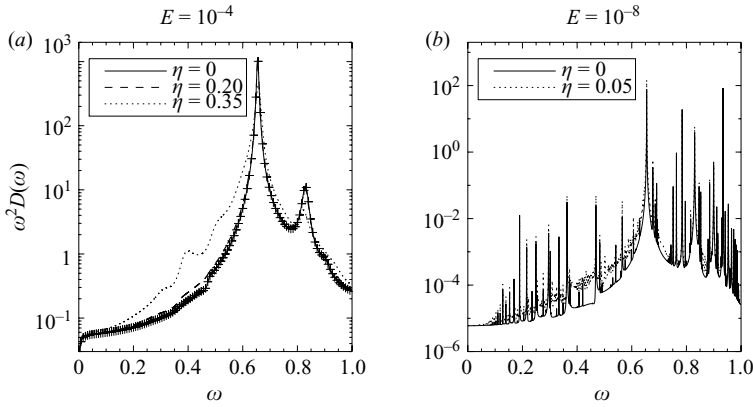
$E = 10^{-4}$ $E = 10^{-8}$

(*a*)

(*b*)

FIGURE 18. The resonance curve for various size of the inner core and two Ekman numbers. (*a*) Note that the pluses correspond to the case $\eta = 0.1$ and are almost sitting on the curve $\eta = 0$; the difference is always less than two percents. (*b*) The same scan at a much lower, but more realistic Ekman number. A small core induces important differences.
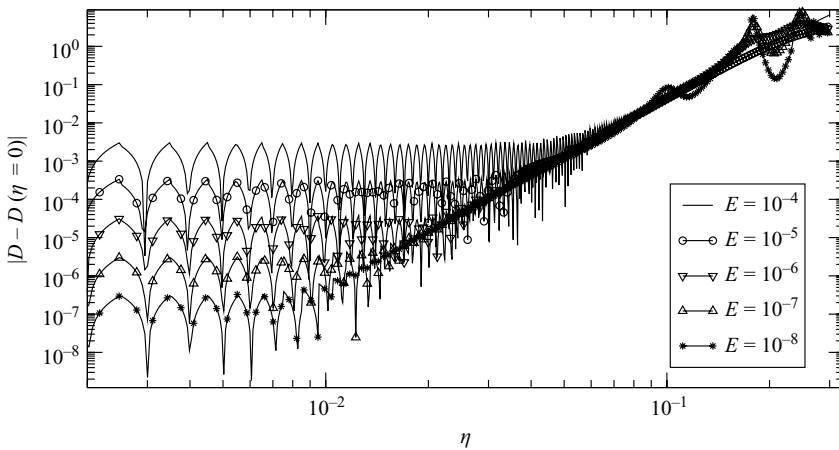
FIGURE 19. Variations of the dissipation at a given Ekman number for varying sizes of the inner core. The frequency of the forcing has been arbitrarily fixed to $\omega = 0.55$.

To be more quantitative and determine the threshold η_c, for a given E, beyond which the core cannot be ignored, we computed the dissipations at various E, keeping ω fixed and varying the size of the inner core. The curves in figure 19 illustrate these variations of the dissipation. They have been computed for $\omega = 0.55$ but the behaviour seems to be generic: We picked up two other frequencies and found the same trends. However, for $\omega = \sqrt{3/7}$, which is the broad resonance showing up in figure 18(*b*) and which corresponds to a large-scale mode of the full sphere (e.g. Greenspan 1969), we do not find this behaviour.

From the curves in figure 19, we could determine that for sufficiently small η

$$D(\eta) = D(\eta = 0) + a(\eta)E + b\eta^5, \tag{3.3}$$

where $D(\eta)$ is the viscous dissipation, b is a constant and $a(\eta)$ is a rapidly varying piecewise bounded linear function. The E-dependence is expected from a flow which does not (or little) depend on the viscosity as it is the case for the full sphere

modes. The η^5-dependence can be, tentatively, explained using the solution derived in Rieutord (1991) (see the discussion in Appendix C). From the law (3.3) we therefore conclude that the inner core influences the dissipation when $b\eta^5 \geqslant a_m E$, a_m being the upper bound of $a(\eta)$, showing that the critical radius of the inner core is

$$\eta_c = q E^{1/5}, \tag{3.4}$$

where the coefficient q weakly depends on the frequency of the forcing. We find $q \sim 0.4$. This formula shows that only extremely small cores can be neglected in realistic conditions where $E \lesssim 10^{-8}$.

3.7. *Discussion*

The foregoing results show that the three-dimensional flows are significantly different from their two-dimensional counter part. The numerical solutions show a kind of exchange of the roles between the attractors and the critical latitude singularities as one shifts from the two-dimensional to the three-dimensional problem. In two dimensions the attractors are clearly dominating the dynamics and control the periodically forced flows. The shear layer emitted at the critical latitude is present but not essential. In three dimensions we observe the opposite: the shear layer emitted at the critical latitude on the inner sphere plays a crucial role in the fluid's response to the periodic forcing, while attractors appear when they are 'fed' by this shear layer.

We have no definite explanation to this observation. We conjecture that it is a consequence of two modifications in the solutions when one changes the dimension of the problem. The first may come from the different Riemann functions of the two- and three-dimensional problems. We recall that the general solution of a hyperbolic problem may be expressed as

$$\Pi(S) = \frac{1}{2}(\Pi(P) + \Pi(Q)) + \frac{1}{2} \int_{PQ} R(S, M) \left(\frac{\partial \Pi}{\partial u_+} \, \mathrm{d}u_+ - \frac{\partial \Pi}{\partial u_-} \, \mathrm{d}u_- \right)$$
$$+ \Pi(M) \left(\frac{\partial R}{\partial u_+} \, \mathrm{d}u_+ - \frac{\partial R}{\partial u_-} \, \mathrm{d}u_- \right), \tag{3.5}$$

where $R(S; M)$ is the Riemann function associated with the Poincaré operator; integration is done on the data line PQ. In two-dimensional this function is a combination of a Dirac distribution and the identity, while in three-dimensional it is a Legendre function (see Rieutord *et al.* 2001). Hence, in two-dimensional, a singularity on the data line will remain on the web of characteristics issued from this point, while in three-dimensional it may generate singular points outside this web. Thus, the influence of the critical latitude singularity in the three-dimensional problem is likely stronger than in the two-dimensional one.

The second modification brought about by the third dimension is the boundary of the domain. While in two-dimensional the true fluid domain is a disk with a core, which is not a simply connected fluid domain, in three-dimensional the meridional section of the fluid layer is a simply connected domain. The difference comes from the presence of the rotation axis which is a line of the meridional plane where the characteristics must reflect, which is not the case in two-dimensional. We conjecture that this difference makes the eventual existence of fundamental intervals (introduced by Maas & Lam 1995), more difficult thus making the excitation of shear layers along the attractors also more difficult.

4. Conclusions

To conclude this work, we may summarize our results in the following way. First, it turns out that the two-dimensional model, which is equivalent to the section of a slender (cored) torus, is well understood:

(i) The dissipation curve is very spiky as one scans the frequency axis and each spike corresponds to a resonance. This resonance is associated with a frequency for which the Lyapunov exponent is zero. We have shown that in most cases the flow is associated with an attractor whose shear layer width scales as $E^{1/4}$. In a few cases, when the frequency of the forcing is of the form $\sin(p\pi/2q)$, where p and q are integers, the resonance is stronger, but narrower, and corresponds to one of the few eigenmodes which remain when an inner core is inserted at the centre of a circular domain.

(ii) In between resonances, which are not dense (but have accumulation points), the dissipation reaches a constant value at vanishing viscosity, as predicted by Ogilvie (2005).

The two-dimensional model thus offers a rather neat picture well constrained by the analytical results. It shows that, contrary to previous expectations, dissipation is very sensitive to viscosity, essentially because of resonances but also because, outside resonances, shear layers associated with different attractors reach their asymptotic regime at very different Ekman numbers.

In three dimensions, results show some similarities with the two-dimensional model but also major differences. Among the similarities, we note that the dissipation curve is very spiky too. There also exist intervals of frequencies where the dissipation does not depend on viscosity when this quantity is low enough. There are also resonances where the dissipation seems to increase without bounds when the viscosity vanishes.

However, there are major differences. First, we observed that the critical latitude singularity on the inner sphere plays a major role in the response of the fluid to the forcing. It is systematically emitting a shear layer. Using the scalings of the Ekman layer at this place, we could explain the vanishing dissipation with vanishing viscosity when the frequency of the forcing is associated with a periodic orbit of characteristics. The latter case also stresses another difference: whereas in the two-dimensional case these periodic orbits were associated with strong and narrow resonances, in the three-dimensional case they are associated with antiresonances: the dissipation vanishes with the viscosity (following a $E^{2/5}$ law).

We observed that in the two-dimensional case, least damped modes are associated with frequencies where the Lyapunov exponent is zero. In three dimensions, such an association also exists but some of the least damped modes are also found in association with intervals of frequencies where the mapping is weakly contracting (because of long-period attractors). Our numerical results on the forced problem show that only this latter kind of least damped modes lead to strong resonances. The question of whether these resonances can reach an asymptotic regime remains open; the fractal nature of the Lyapunov exponents in the frequency region where they exist may prevent any asymptotic limit. Clearly, for one of them, even at $E = 10^{-11}$, the asymptotic regime is not reached. The close examination of this resonance has nevertheless shown that some intermediate regimes may exist when attractors of very long period cover the same intervals of frequencies as the resonances. Such regimes are astrophysically relevant and deserve more investigations.

Unfortunately and unlike in the two-dimensional case, we have little analytical guide in the three-dimensional case. Tentatively, we interpreted the striking role of the characteristics emitted at the critical latitude as a consequence of the nature of the

Riemann function associated with the Poincaré operator and the probable different fundamental intervals associated with the mapping of characteristics.

Finally, the striking general conclusion is that a periodically forced flow in a spherical shell is quite different from what can be expected from a simple response of resonant eigenmodes. Previous work has shown that eigenmodes were often featured by attractors of characteristics, but those modes turned out to be of little interest for the forced problem. Interestingly enough, the dissipation curve reveals some parts of the pseudospectrum of the Poincaré operator, thus offering another way to investigate the properties of this operator.

The solutions that we computed also showed that the critical latitude singularity is a determinant feature of the periodically forced flows. More work is now needed to fully understand the interplay of the singularities generated by both the critical latitude and the attractors of characteristics. We note that Goodman & Lackner (2009), while examining the tidal response of a Jovian planet, were also led to the conclusion that the critical latitude at the interface between a solid core and a fluid envelope plays a crucial role in the dissipation of kinetic energy. In this same planetary context, we showed that planets with a very small core could be assimilated to a full sphere only when the relative radius of the inner core η is less than $0.4E^{1/5}$. Beyond this, usually very small, value the dissipation grows rapidly with the core size as η^5.

To conclude on the astrophysical problem, which motivated this study, our results stress the importance of viscosity. They unfortunately remove the possibility, envisaged by Ogilvie & Lin (2004), that the synchronization time scale of binary stars be independent of the viscosity, which is usually not a well known quantity.

Appendix A. Viscous dissipation in the slender torus

A.1. *Equivalence of coordinate systems*

Using non-dimensional variables, viscous dissipation is

$$D = \frac{E}{2} \int_{(V)} |c|^2 \, dV,$$

where $|c|$ symbolizes the norm of the shear tensor. In usual cylindrical coordinates, this norm reads

$$|c|^2 = c_{ij}c_{ij}^* = |c_{ss}|^2 + |c_{\varphi\varphi}|^2 + |c_{zz}|^2 + 2(|c_{s\varphi}|^2 + |c_{sz}|^2 + |c_{\varphi z}|^2)$$

with

$$c_{ss} = 2\frac{\partial v_s}{\partial s}, \quad c_{\varphi\varphi} = 2\left(\frac{1}{s}\frac{\partial v_\varphi}{\partial \varphi} + \frac{v_s}{s}\right), \quad c_{zz} = 2\frac{\partial v_z}{\partial z},$$

$$c_{s\varphi} = \frac{1}{s}\frac{\partial v_s}{\partial \varphi} + \frac{\partial v_\varphi}{\partial s} - \frac{v_\varphi}{s}, \quad c_{sz} = \frac{\partial v_z}{\partial s} + \frac{\partial v_s}{\partial z}, \quad c_{\varphi z} = \frac{\partial v_\varphi}{\partial z} + \frac{1}{s}\frac{\partial v_z}{\partial \varphi}.$$

Considering axisymmetric solutions at $s \gg 1$, the shear tensor components simplify into

$$c_{ss} = 2\frac{\partial v_s}{\partial s}, \quad c_{\varphi\varphi} = 0, \quad c_{zz} = 2\frac{\partial v_z}{\partial z},$$

$$c_{s\varphi} = \frac{\partial v_\varphi}{\partial s}, \quad c_{sz} = \frac{\partial v_z}{\partial s} + \frac{\partial v_s}{\partial z}, \quad c_{\varphi z} = \frac{\partial v_\varphi}{\partial z}.$$

Using the meridional stream function ψ, we may further write

$$c_{zz} = 2\frac{\partial^2 \psi}{\partial s \partial z} = -c_{ss}, \quad c_{sz} = \frac{\partial^2 \psi}{\partial s^2} - \frac{\partial^2 \psi}{\partial z^2} \quad c_{s\varphi} = \frac{\partial u}{\partial s}, \quad c_{\varphi z} = \frac{\partial u}{\partial z}$$

So that the volumic dissipation is:

$$|c|^2 = 2(|c_{ss}|^2 + |c_{s\varphi}|^2 + |c_{sz}|^2 + |c_{\varphi z}|^2).$$

Now a direct calculation shows that

$$c_{zz} = \sin 2\phi \left(\psi_{\rho\rho} - \psi_\rho/\rho - \psi_{\phi\phi}/\rho^2\right) + \frac{2\cos 2\phi}{\rho}(\psi_{\rho\phi} - \psi_\phi/\rho) = -c_{ss}$$

and

$$c_{sz} = \cos 2\phi(\psi_{\rho\rho} - \psi_\rho/\rho - \psi_{\phi\phi}/\rho^2) - \frac{2\sin 2\phi}{\rho}(\psi_{\rho\phi} - \psi_\phi/\rho),$$

where we recognize the expressions of $c_{\rho\rho}$ and $c_{\rho\phi}$ of (mr). Thus,

$$c_{zz} = -c_{ss} = \sin 2\phi c_{\rho\phi} + \cos 2\phi c_{\rho\rho},$$
$$c_{sz} = \cos 2\phi c_{\rho\phi} - \sin 2\phi c_{\rho\rho}.$$

In the same way, we also find that

$$c_{s\phi} = \cos\phi c_{\rho\zeta} - \sin\phi c_{\phi\zeta} \quad \text{and} \quad c_{\phi z} = \sin\phi c_{\rho\zeta} + \cos\phi c_{\phi\zeta},$$

which leads to

$$|c|^2 = 2(|c_{\rho\rho}|^2 + |c_{\rho\zeta}|^2 + |c_{\phi\zeta}|^2 + |c_{\rho\phi}|^2)$$

as expected.

A.2. *Dissipation as function of the Fourier components*

We first note that

$$\int_0^{2\pi} |c_{\rho\zeta}|^2 + |c_{\theta\zeta}|^2 \, d\theta = 2\pi \sum_n |V_n'|^2 + \frac{n^2}{\rho^2}|V_n|^2,$$

$$\int_0^{2\pi} |c_{\rho\rho}|^2 \, d\theta = 2\pi \sum_n \left|\frac{2n}{\rho}\left(\psi_n' - \frac{\psi_n}{\rho}\right)\right|^2,$$

$$\int_0^{2\pi} |c_{\rho\theta}|^2 \, d\theta = 2\pi \sum_n \left|\psi_n'' - \frac{\psi_n'}{\rho} + \frac{n^2\psi_n}{\rho^2}\right|^2.$$

Since the total dissipation is

$$D = E \int_{(V)} (|c_{\rho\rho}|^2 + |c_{\rho\zeta}|^2 + |c_{\theta\zeta}|^2 + |c_{\rho\theta}|^2) \, dV,$$

it finally expresses as

$$D = 2\pi E \int_{\eta}^{1} \left\{ \sum_{n} |V_n'|^2 + \frac{n^2}{\rho^2}|V_n|^2 + \left| \frac{2n}{\rho} \left(\psi_n' - \frac{\psi_n}{\rho} \right) \right|^2 + \left| \psi_n'' - \frac{\psi_n'}{\rho} + \frac{n^2 \psi_n}{\rho^2} \right|^2 \right\} \rho \, \mathrm{d}\rho.$$

If the solutions are equatorially symmetric $V_{-n} = V_n$ and $\psi_{-n} = -\psi_n$, so that

$$D = 4\pi E \int_{\eta}^{1} \left\{ \frac{1}{2}|V_0'|^2 + \sum_{n>0} |V_n'|^2 + \frac{n^2}{\rho^2}|V_n|^2 + \left| \frac{2n}{\rho} \left(\psi_n' - \frac{\psi_n}{\rho} \right) \right|^2 \right.$$
$$\left. + \left| \psi_n'' - \frac{\psi_n'}{\rho} + \frac{n^2 \psi_n}{\rho^2} \right|^2 \right\} \rho \, \mathrm{d}\rho.$$

Appendix B. Influence of boundary conditions

Fotheringham & Hollerbach (1998) studied the influence of boundary conditions (no-slip or stress-free) on the inertial modes of a spherical shell. They found that this influence was very small. In the forced flow that we study here, this is also the case. The contribution to dissipation of Ekman layers that appear if no-slip boundary conditions are used may be estimated as follows: In the case of the asymptotic regime where the fluid flow is following an attractor, the velocity scales as $E^{-1/3}$ (Ogilvie 2005) and the boundary layer velocity gradients $\partial u / \partial x$ are $O(E^{-1/3}/E^{1/2}) = O(E^{-5/6})$. However, the volume occupied by the boundary layers is $O(E^{5/6})$, thus, the resulting dissipation scales like $E^{1/6}$ which is very small compared to the contribution of the internal shear layers, which is unity. In the case of the resonances of the two-dimensional slender torus, which are associated with shear layers of width scaling in $E^{1/4}$, the contribution of Ekman layers is even weaker, namely $O(E^{1/4})$. It is only in the case of the regular modes of the torus, that a strong effect is noticed, as expected. However these modes do not exist in the more realistic set-up of a spherical shell: we obtained singular solution (the 'antiresonances' see § 3.3). In this case we find that the dissipation scales like $E^{2/5}$, which seems to be also the case when a no-slip boundary condition is used on the inner core.

Appendix C. The asymptotic law for cores of vanishing sizes

We may recover the dependence in η^5 of the viscous dissipation when $\eta \ll 1$ by considering the solutions found by Rieutord (1991). Indeed, in this paper it was shown that an oscillatory flow in a rotating background with spherical symmetry could be described by two kinds of solutions when these are decomposed onto the spherical harmonic basis. These solutions (in fact the radial functions of each spherical harmonic component) are either of Bessel or polynomial type. The Bessel type solutions describe the boundary layer regions, while the polynomials describe the flow in the remaining volume.

Considering the inviscid case, we shall focus on the polynomial solutions. Rieutord (1991) has shown that these solutions also split into two categories: one is regular at the origin, the other is regular at infinity. The first one is easily related to the inertial modes of the full sphere which have been found by Bryan (1889) (see also Greenspan 1969; Rieutord 1997). They are exact solutions of the inviscid problem at eigenfrequencies. Below, we shall refer to these solutions as class-one solutions.

The second class of solutions are those with radial functions with polynomials in $1/r$ that are regular at infinity. However, unlike those regular at the origin, these solutions are exact only when the momentum equation is expanded on a finite number of spherical harmonics, namely when the series is artificially truncated at a given maximum order, just like in a numerical calculation. This is expected since the solutions regular at infinity are singular at the critical latitude on an inner bounding sphere (see Rieutord *et al.* 2001). Below, we refer to these solutions as class-two solutions.

Now if we think to the solutions in their spherical harmonic decomposition, we note that the radial velocity of the class-one solution is dominated near the centre by its $u^2 Y_2$ component (we restrict the discussion to the axisymmetric and equatorially symmetric flows). This is because $u^{\ell} \sim r^{\ell-1}$ as $r \to 0$. When a small inner core is introduced in the inviscid problem, we need to add solutions that are regular at infinity so that the inner boundary condition $u_r(\eta) = 0$ is met. This is the usual procedure in regular elliptic problems like the Poisson problem for instance. However, in the Poincaré problem, this cannot be done because the class-two solutions are singular. However, if we restrict our problem to a finite number of spherical harmonics (which is a way of regularization), we can use this kind of solutions.

As shown in Rieutord (1991), the form of class-two solutions for $u^2(r)$ is in r^{-4}. If we write

$$\boldsymbol{u} = \boldsymbol{u}_0 + \alpha_2 \boldsymbol{u}_\infty^2 + \alpha_4 \boldsymbol{u}_\infty^4 + \cdots,$$

where $\boldsymbol{u}_0$ is the class-one solution and $\boldsymbol{u}_\infty^J$ are the class-two solution of order J (their lowest order is $u^J(r) = r^{-J}$). Imposing that $u_r(\eta) = 0$ for $\eta \ll 1$, we easily find that α_2 is $O(\eta^5)$ and that more generally, α_{2p} is $O(\eta^{2p+3})$.

Hence, to leading order, we may write

$$\boldsymbol{u} = \boldsymbol{u}_0 + \eta^5 \boldsymbol{u}_\eta. \tag{C 1}$$

Although the truncated solutions are not exact, we know that viscosity will, in the end, also truncate the spherical harmonics series. Computing the viscous dissipation from (C 1) shows that

$$D(\eta) = D(\eta = 0) + \eta^5 D_1,$$

where the D_1 term might depend on the Ekman number. Although quite close to the searched expression (3.3), this equation misses the $a(\eta)E$ term and the fact that D_1 seems to be independent of E.

We note that the critical latitude boundary layer on the inner sphere could induce a velocity field which is $O(\eta/E^{1/5})$. This scaling also suggests that a transition occurs when $\eta \sim E^{1/5}$. This latter remark shows that the complete explanation is likely involved and a more detailed analysis is necessary to fully understand the intricacy of the limits $\eta \to 0$ and $E \to 0$.

REFERENCES

BRYAN, G. 1889 The waves on a rotating liquid spheroid of finite ellipticity. *Phil. Trans. R. Soc. Lond.* **180**, 187–219.

DINTRANS, B. & RIEUTORD, M. 2000 Oscillations of a rotating star: a non-perturbative theory. *A&A* **354**, 86–98.

DINTRANS, B., RIEUTORD, M. & VALDETTARO, L. 1999 Gravito-inertial waves in a rotating stratified sphere or spherical shell. *J. Fluid Mech.* **398**, 271–297.

FOTHERINGHAM, P. & HOLLERBACH, R. 1998 Inertial oscillations in a spherical shell. *Geophys. Astrophys. Fluid Dyn.* **89**, 23–43.

GERKEMA, T., ZIMMERMAN, J. T. F., MAAS, L. R. M. & VAN HAREN, H. 2008 Geophysical and astrophysical fluid dynamics beyond the traditional approximation. *Rev. Geophys.* **46**, RG2004.

GIURICIN, G., MARDIROSSIAN, F. & MEZZETTI, M. 1984 Synchronization in eclipsing binary stars. *A&A* **131**, 152–158.

GOODMAN, J. & LACKNER, C. 2009 Dynamical tides in rotating planets and stars. *ApJ* **696**, 2054–2067.

GREENSPAN, H. P. 1969 *The Theory of Rotating Fluids*. Cambridge University Press.

HOLLERBACH, R. & KERSWELL, R. 1995 Oscillatory internal shear layers in rotating and precessing flows. *J. Fluid Mech.* **298**, 327–339.

KERSWELL, R. 1995 On the internal shear layers spawned by the critical regions in oscillatory Ekman boundary layers. *J. Fluid Mech.* **298**, 311–325.

KERSWELL, R. R. 2002 Elliptical instability. *Annu. Rev. Fluid Mech.* **34**, 83–113.

LACAZE, L., LE GAL, P. & LE DIZÈS, S. 2005 Elliptical instability of the flow in a rotating shell. *Phys. Earth Planet. Inter.* **151**, 194–205.

MAAS, L. 2001 Waves focusing and ensuing mean flow due to symmetry breaking in rotating fluids. *J. Fluid Mech.* **437**, 13–28.

MAAS, L. & HARLANDER, U. 2007 Equatorial wave attractors and inertial oscillations. *J. Fluid Mech.* **570**, 47–67.

MAAS, L. & LAM, F.-P. 1995 Geometric focusing of internal waves. *J. Fluid Mech.* **300**, 1–41.

MANASSEH, R. 1996 Nonlinear behaviour of contained inertia waves. *J. Fluid Mech.* **315**, 151–173.

MAZEH, T. 2008 Observational evidence for tidal interaction in close binary systems. In *EAS Publications Series* (ed. M.-J. Goupil & J.-P. Zahn), vol. 29, pp. 1–65.

OGILVIE, G. 2005 Wave attractors and the asymptotic dissipation rate of tidal disturbance. *J. Fluid Mech.* **543**, 19–44.

OGILVIE, G. 2009 Tidal dissipation in rotating fluid bodies: a simplified model. *MNRAS* **396**, 794–806.

OGILVIE, G. I. & LIN, D. N. C. 2004 Tidal dissipation in rotating giant planets. *ApJ* **610**, 477–509.

RIEUTORD, M. 1987 Linear theory of rotating fluids using spherical harmonics. I. Steady flows. *Geophys. Astrophys. Fluid Dyn.* **39**, 163.

RIEUTORD, M. 1991 Linear theory of rotating fluids using spherical harmonics. II. Time periodic flows. *Geophys. Astrophys. Fluid Dyn.* **59**, 185–208.

RIEUTORD, M. 1997 *Une introduction à la dynamique des fluides*. Masson.

RIEUTORD, M., GEORGEOT, B. & VALDETTARO, L. 2000 Waves attractors in rotating fluids: a paradigm for ill-posed cauchy problems. *Phys. Rev. Lett.* **85**, 4277–4280.

RIEUTORD, M., GEORGEOT, B. & VALDETTARO, L. 2001 Inertial waves in a rotating spherical shell: attractors and asymptotic spectrum. *J. Fluid Mech.* **435**, 103–144.

RIEUTORD, M. & VALDETTARO, L. 1997 Inertial waves in a rotating spherical shell. *J. Fluid Mech.* **341**, 77–99.

RIEUTORD, M., VALDETTARO, L. & GEORGEOT, B. 2002 Analysis of singular inertial modes in a spherical shell: the slender toroidal shell model. *J. Fluid Mech.* **463**, 345–360.

ROBERTS, P. & STEWARTSON, K. 1963 On the stability of a Maclaurin spheroid of small viscosity. *ApJ* **137**, 777–790.

ROCCA, A. 1987 Forced oscillations in a rotating star: low frequency gravity mode. *A&A* **175**, 81–90.

ROCCA, A. 1989 Tidal effects in rotating close binaries. *A&A* **213**, 114–126.

SAVONIJE, G. J. & WITTE, M. G. 2002 Tidal interaction of a rotating 1 $M_\odot$ star with a binary companion. *A&A* **386**, 211–221.

STEWARTSON, K. 1971 On trapped oscillations of a rotating fluid in a thin spherical shell. *Tellus* **23**, 506–510.

TILGNER, A. 1999 Driven inertial oscillations in spherical shells. *Phys. Rev.* D **59**, 1789.

TREFETHEN, L. & EMBREE, M. 2005 *Spectra and Pseudospectra*. Princeton University Press.

VALDETTARO, L., RIEUTORD, M., BRACONNIER, T. & FRAYSSE, V. 2007 Convergence and round-off errors in a two-dimensional eigenvalue problem using spectral methods and arnoldi-chebyshev algorithm. *J. Comput. Appl. Math.* **205**, 382–393.

WITTE, M. G. & SAVONIJE, G. J. 1999a The dynamical tide in a rotating $10 M_\odot$ main sequence star. A study of g- and r-mode resonances. *A&A* **341**, 842–852.

WITTE, M. G. & SAVONIJE, G. J. 1999b Tidal evolution of eccentric orbits in massive binary systems. A study of resonance locking. *A&A* **350**, 129–147.

WITTE, M. G. & SAVONIJE, G. J. 2001 Tidal evolution of eccentric orbits in massive binary systems. II. Coupled resonance locking for two rotating main sequence stars. *A&A* **366**, 840–857.

ZAHN, J.-P. 1966 Les marées dans une étoile double serrée. *Annales d'Astrophysique* **29**, 313, 489, 565.

ZAHN, J.-P. 1975 The dynamical tide in close binaries. *A&A* **41**, 329–344.

ZAHN, J.-P. 1977 Tidal friction in close binaries. *A&A* **57**, 383–394.

ZAHN, J.-P. 1992 Circulation and turbulence in rotating stars. *A&A* **265**, 115.

ZAHN, J.-P. 2008 Tidal dissipation in binary systems. In *EAS Publications Series* (ed. M.-J. Goupil & J.-P. Zahn), vol. 29, pp. 67–90.

ZHANG, K. 1994 On coupling between the Poincaré equation and the heat equation. *J. Fluid Mech.* **268**, 211–229.

ZHANG, K. 1995 On coupling between the Poincaré equation and the heat equation: non-slip boundary condition. *J. Fluid Mech.* **284**, 239–256.